Atmospheric
Chemistry
and Physics
Discussions

Response of particle number concentrations to Clean Air Action: Lessons from the first long-term aerosol measurements in a typical urban valley, West China

Suping Zhao [a,b,c], Ye Yu [a,b], Jianglin Li [a,b], Daiying Yin [d,e], Shaofeng Qi [a,e], Dahe Qin [c]

5   [a] Key Laboratory of Land Surface Process and Climate Change in Cold and Arid Regions, Northwest Institute of Eco-Environment and Resources, Chinese Academy of Sciences, Lanzhou 730000, China
[b] Pingliang Land Surface Process & Severe Weather Research Station, Pingliang, 744015, China
[c] State Key Laboratory of Cryospheric Science, Northwest Institute of Eco-Environment and Resources, Chinese Academy of Sciences, Lanzhou 730000, China

10   [d] Key Laboratory of Desert and Desertification, Northwest Institute of Eco-Environment and Resources, Chinese Academy of Sciences, Lanzhou 730000, China
[e] University of Chinese Academy of Sciences, Beijing 100049, China

Correspondence to: Suping Zhao (zhaosp@lzb.ac.cn); Ye Yu (yyu@lzb.ac.cn)

Abstract. The strictest ever Clean Air Action (CAA) has been implemented by Chinese government

15   since 2013 to alleviate the severe haze pollution. The $PM_{2.5}$ mass concentration was found to be largely reduced in response to emission mitigation policies, but response of particle number concentrations (PNCs) to CAA was less evaluated in the previous studies, which may be largely different from $PM_{2.5}$ mass due to newly formed particle impacts. In this work, the first *in-situ* observation of particle number size distributions (PNSDs) during 2012-2019 in urban Lanzhou was used to analyze long-term PNCs

20   variations and CAA impacts. The average number of particles in nucleation (N_{13-25}, particle number in the size range of 13-25 nm), Aitken (N_{25-100}, particle number in the size range of 25-100 nm) and accumulation ($N_{100-800}$, particle number in the size range of 100-800 nm) modes were respectively 2514.0 cm^{-3}, 10768.7 cm^{-3}, and 3258.4 cm^{-3}, and N_{25-100} accounted for about 65.1% of total PNCs during the campaign. K-means clustering technique was used to classify the hourly mean PNSDs into

25   six clusters, and each cluster corresponded to a specific source and influencing factor. The polluted clusters governed the winter PNCs before 2016, and their occurrence was less and less frequent after 2016, which was largely dominated by reduction in primary emissions. However, the contribution of new particle formation (NPF) events to summer N_{13-25} decreased from 50% to about 10% during 2013 to 2015, and then increased to reach around 60% in 2019. The trends of size-resolved PNCs for each

30   cluster were quantified by Theil-Sen regression. The size-segregated PNCs exhibited downward trends for all clusters during 2012-2015, especially in spring. The annual relative slopes of spring PNCs varied

from -54.7% to -17.2%, -42.6% to -14.1%, and -40.7% to -17.5% per year for 13-25, 25-100, and

100-800 nm size ranges, and the reduction in the polluted clusters was much larger than NPF clusters.

The ultrafine particle number was increased and the amplitude was much greater during 2016-2019.

The annual relative slopes of N_{13-25} varied between 8.0% in fall and 135.5% in spring for NPF cluster.

5   In response to CAA, the increased daytime net radiation, higher ambient temperature and lower relative

humidity at noon for NPF events also could partly explain the higher N_{13-25} induced by the more

frequent nucleation events after 2016, especially in spring. The air mass were mainly from the adjacent

regions of urban Lanzhou and less affected by long-range transport for NPF events, and the thus

particles were not easily grown by coagulation during transport processes, which was helpful for

10   occurrence of NPF events. Therefore, some effective control measures cooperatively controlled particle

number and mass should be took for the Chinese megacities.

15

20

1 Introduction

China has been experienced large-scale and long-lasting winter haze pollution due to fast-growing

economy and urbanization in past decades. The high concentration of aerosols perturb radiative balance

of the atmosphere and surface by directly scattering and absorbing solar radiation, or indirectly alter

5   cloud optical properties and lifetime serving as condensation nuclei and ice nuclei (Andreae and

Rosenfeld, 2008; Gao et al., 2015; Li et al., 2017). The adverse effect of deteriorated air quality on

public health is of the greatest concern in China (Hu et al., 2017; Lelieveld et al., 2015). The present air

quality standards consider particle mass instead of number concentration (WHO, 2000). However,

compared with the larger aerosol particles, the ultrafine particles (UFPs, diameter < 100 nm) scarcely

10   contribute to aerosol mass, while they share the largest number fraction in urban areas (Hussein et al.,

2004; Wehner et al., 2004). The toxicity of UFPs is enhanced by the large surface area due to high

number concentrations, and they can penetrate deep into lungs, ending up in the blood circulation

(Oberdörster et al., 2005; Schmid and Stoeger, 2016).

15   Aerosol ability to efficiently scatter or absorb light depends not only on their chemical composition but

on their sizes as well (Asmi et al., 2013). Liu et al. (2020) indicated that coating plays an important role

in light absorption. The amplification of black carbon absorption by the coating increased from 1.21 to

1.75 with increasing aerodynamic diameter (D_{ae}) due to the thicker coating of BC-containing particles

with a larger D_{ae}. Their study highlights the strong dependence of the microphysical and optical

20   properties of BC on size. The more recent study of Zhao et al. (2021) found that interdecadal AOD was

negative trend from 2009 to 2018, which may be related to the variation in particle size distribution.

Some aerosol monitoring networks were established around the world for long-term measurements of

climate-relevant aerosol properties, such as Geophysical Monitoring for Climate Change (GMCC,

Bodhaine, 1983) and Global Atmospheric Watch (GAW, Rose et al., 2021). The particle number

25   concentration (PNCs) and size distributions (PNSDs), considered to be a primary indicator of human

impacts on atmospheric composition, was the main aerosol property measured at the networks. Based

on long-term *in-situ* measurements at the network sites, many studies on particle number and size

distributions have been conducted since the 1990s in Europe and North America (Asmi et al., 2011;

Birmili et al., 2016; Dal Maso et al., 2008; Heintzenberg et al., 2011; Krecl et al., 2017; Kulmala et al.,

30   2004; Makela et al., 1997; Sun et al., 2020; Wiedensohler et al., 2012). Their studies indicated that the

Atmospheric
Chemistry
and Physics
Discussions

Open Access
EGU

annual, weekly and diurnal cycles largely depended on station type and geographic location. The more

recent study of Schmale et al. (2018) also well illustrated the importance of measuring the PNSD over

long enough time periods in contrasting micro-environments for the understanding of aerosol-climate

interactions and the improvement of their representation in numerical models. Sun et al. (2020)

5   determined long-term trends of PNCs during 2009-2018 for 16 sites ranging from roadside to high

Alpine environments, and the annual relative slope varied from -17.2% to -1.7%, -7.8% to -1.1%, and

-11.1% to -1.2% per year for 10-30 nm, 30-200 nm and 200-800 nm size bins, respectively. The

downward trends of PNCs were found to be dominated by the reductions in various anthropogenic

emissions, while meteorology impacts were less important or negligible. However, a few long-term

10   PNSD measurements in the developing countries mainly concentrated on urban Beijing since 2004

(Wang et al., 2013; Wehner et al., 2004), the North China Plain since 2008 (Shen et al., 2011), and

Mount Waliguan since 2005 (Kivekas et al., 2009). Aitken mode particles (25-100 nm) were found to

be accounted for about half of total PNCs in urban areas in China (Wu et al., 2008), and number in

accumulation mode (100-1000 nm) was around 4 times higher than that in the developed countries

15   (Wehner et al., 2008; Wu et al., 2008), indicating that largely different PNSD characteristics in China

from Europe and North America.

PM$_{2.5}$ (particulate matter with aerodynamic diameter less than 2.5 μm) decreased by 30%-50% across

China over the 2013-2018 period in response to Air Pollution Prevention and Control Action Plan

20   (APPCAP) in 2013 implemented by Chinese central government (Zhai et al., 2019). Compared with

PM$_{2.5}$ mass concentrations, the particle number concentrations were more directly affected by newly

formed particles (Dal Maso et al., 2008; Dinoi et al., 2021), and new particle formation (NPF) events

contributed about 54% of total PNCs in Leipzig, Germany (Ma and Birmili, 2015). Guo et al. (2014)

tried to reveal the causal connection between NPF and haze pollution, and reported that NPF trends to

25   precede winter haze episodes in Beijing. The more recent study by Kulmala et al. (2021) found that

over 65% of the number concentrations of haze particles resulted from NPF events in Beijing, and their

findings suggested that almost all present-day haze episodes originated from NPF, mainly since

primary emission considerably decreased during recent year. PNSDs were considered to be better

indicators of the strength of emission sources (Vu et al., 2015), but they were more easily modulated by

30   aerosol dynamic processes, such as nucleation, coagulation, volatilisation and condensations (Birmili et

al., 2010; Kulmala, 2003). Nucleation and coagulation were largely affected by coagulation sink (CoagS), and CoagS significantly decreased due to large reduction of $PM_{2.5}$ mass concentrations in response to APPCAP. Therefore, response of particle number concentration in different size bins to emission mitigation policies may be different from $PM_{2.5}$ mass concentration.

5

The long-term PNSDs measurements were mainly conducted before APPCAP in China, and it has been less reported that the response of particle number concentrations to the strictest ever air pollution control policies implemented by Chinese central government. Lanzhou, as one of the most polluted cities around the world at special basin terrain, obtained Today's Transformative Step 2015 awarded by

10 the United Nations due to significant improvement in urban air quality (Zhao et al., 2018). The atmospheric horizontal and vertical dispersion conditions inside the basin are poor due to weak winds and strong multi-layer temperature inversion induced by basin terrain (Pandolfi et al., 2014). Therefore, the air pollutants were easily trapped inside the basin and hard to disperse to the upper air. Furthermore, basin aerosol pollution was largely controlled by vertical than horizontal dispersion as compared to the

15 plain (Zhao et al., 2019). Based on a unique PNSD dataset for the period of 2012-2019 at urban Lanzhou in West China, this study investigates the long-term trends of PNCs in different modes, to evaluate the role of emission reduction and meteorology in PNC variations. The results of this study may be important for the policymakers to cooperatively prevent and control heavy particle mass and number concentrations in Chinese megacities.

20

2 Data and methods

2.1 Measurement site descriptions

Lanzhou, located at the intersection of Tibetan Plateau, Losses Plateau and Mongolia Plateau, is in a long valley running from the east to the west. The urban area is encircled by the hills rising from 200 m

25 to 600 m, and thus formed saddle-shaped basin terrain (Figure 1). The weak winds and multi-layer temperature inversion occurred frequently due to terrain impacts, and thus the air pollutants are trapped inside the basin (Chu et al., 2008). It was thought to be one of the most polluted cities around the world (WHO, 2014), and photochemical smog episode (PSE) was observed in the 1980s at Xigu District of urban Lanzhou, which was the first time PSE was observed in China (Chen et al., 1986). The

30 observation campaign was conducted from September 2012 to August 2019 on the rooftop of a 32-m

high research building of the Northwest Institute of Eco-Environment and Resources (NIEER), Chinese

Academy of Sciences. There are two major roads with traffic volume more than 2000 cars per hour

near the observation site (Figure 1). The NIEER is surrounded by residential and commercial buildings,

and there are no local industrial sources around the site (Zhao et al., 2015a), and thus the measurement

5   site can represent urban background.

2.2 PNSD, criteria air pollutants and meteorology data

5-min particle number concentrations and size distributions (13-800 nm) were measured continuously

by scanning mobility particle sizer (Model 3936, TSI, USA) for about 7 years at the urban site from

10   September 2012 to August 2019. The aerosol and sheath flowrates were set to 0.3 L min^{-1} and 3 L min^{-1},

respectively. The sampling inlet was mounted 1.5 m above the rooftop. The diffusional and

gravitational losses for the inlet lines of SMPS were calibrated during the campaign. The SMPS's

mobility was calibrated with monodisperse aerosols prior to their deployment in the field. The impactor

was cleaned every day and aerosol and sheath rates were examined with a bubble flow meter to insure

15   the good performance of the instrument. The each PNSD was parameterized with a least-square

log-normal fitting method providing parameters of 2-3 log-normal modes (Birmili et al., 2001). Three

modes (i = 1, 2, 3) were used corresponding to the nucleation mode (13-25 nm), Aitken mode (25-100

nm) and accumulation mode (100-800 nm), respectively. The log-normal distribution is expressed as

(Seinfeld and Pandis, 2006):

$$\frac{dN}{d\log D_p} = \sum_{i=1}^{n} \frac{N_i}{\sqrt{2\pi}\log\sigma_i} \exp\left(-\frac{\left(\log D_p - \log \overline{D}_{p,i}\right)^2}{2\left(\log\sigma_i\right)^2}\right) \qquad (1)$$

where N_i is the total number concentration of the mode i, $\overline{D}_{p,i}$ is the median diameter of mode i, σ_i is

the geometric mean standard deviation of the distribution and n is the number of the modes. The

symbol of log means log10 in this study.

25   The hourly averaged concentrations of the criteria air pollutants (PM$_{2.5}$, PM$_{10}$, SO$_2$, NO$_2$, O$_3$, CO) were

measured at Lanzhou Biologicals Institute, which is around 2.8 km away from the observation site. SO$_2$,

NO$_2$, CO and O$_3$ are measured by the ultraviolet fluorescence method, the chemiluminescence method,

the non-dispersive infrared absorption method and the UV-spectrophotometry method, respectively.

PM$_{2.5}$ and PM$_{10}$ are measured by micro oscillating balance method. Aerosol optical parameters (AOD and Alpha) were measured continuously by a sun tracking spectrophotometer (CE-318, CIMEL, France) during the campaign. The 10-min meteorological parameters including temperature, relative humidity, wind speed and direction, precipitation and raindrop size distribution, and solar radiation were

5 monitored by an automatic meteorological station co-located with the observation site. All the on-line data were hourly averaged and presented at local time (Beijing Time = UTC+8) throughout this paper.

2.3 Trend analysis methods

Referring to the method used in the study of Sun et al. (2020), a customized Sen-Theil trend estimator

10 was used to analyze the long-term trends of PNCs in nucleation, Aitken, and accumulation modes, the concentrations of the criteria air pollutants and meteorological parameters in this study. The technique can calculate the true slope of the parameters by considering the impact of their seasonal, weekly and diurnal cycles, and avoid the effect of outliers and missing values. The change rates for the hourly or daily time series can be calculated with the below equation:

15
$$m_{i,k} = \frac{\left(x\left(i+\Delta t\right) - x\left(i\right)\right)}{\Delta t} \qquad (2)$$

Where k is the integer. Δt is equal to the product of k and 364 days (52 weeks), indicating that data points from two different years are compared only if they were measured in the same hour of the day, day of the week, and season the year.

20 **2.4 Cluster analysis methods**

To extract some more valuable information, K-means clustering method used in various studies has been considered to be a preferred technique for data analysis in environmental fields (Sabaliauskas et al., 2013; Tunved et al., 2004). The K-means clustering routine split the multi-dimensional data into predefined number of subgroups, and clusters are as different as possible from each other, but as

25 homogeneous as possible within themselves, by iteratively minimizing the sum of squared Euclidean distances from each member to its cluster centroid. Cluster analysis was used to divide hourly mean PNSDs during the campaign into several groups with comparable particle number in different size bins within groups. The K-means clustering algorithm available in MATLAB© was used in this study. Based on the rule with maximum inter-cluster and minimum intra-cluster variances, the determination of

number of clusters, a very complicated problem, was conducted by statistical software SAS© in this study, which was given in detail in the study of Zhao et al. (2016).

3 Results and discussion

A continuous 7.5 years dataset was evaluated in this investigation. Except the instrument maintenance and re-location, 80% of the data was effective. The continuous PNSD dataset was integrated to calculate PNCs in different size bins. In this study, diameter ranges for the nucleation mode, Aitken mode, and accumulation mode were determined as 13-25 nm, 25-100 nm, and 100-800 nm, respectively (Dal Maso et al., 2005). The total PNCs covered from 13 nm to 800 nm in mobility diameter.

3.1 Overview of the particle number concentration

Sources and origins of particles in the three modes may be largely varied at a specific micro-environments. Nucleation mode particles are from atmospheric nucleation events which is closely related to the low volatile condensable gases such as water and sulfuric acid and growth of the smaller aerosol particles (Kulmala, 2003). Aitken mode particles are primarily emitted from combustion processes, such as coal combustion for domestic heating in wintertime, and also from hygroscopic growth and coagulation of nucleation mode particles. For relatively clean environment, the growth of nucleation mode particles is predominant due to less coagulation sink (Rose et al., 2021), while the primary emissions are more important at the highly polluted urban areas (Hussein et al., 2004). Accumulation mode particles originate from coagulation and hygroscopic growth of Aitken mode particles and long-range transport from the highly polluted areas.

Figure 2 shows variation of particle number in nucleation mode (N_{13-25}), Aitken mode (N_{25-100}), and accumulation mode ($N_{100-800}$), aerosol optical properties (AOD, Alpha), criteria air pollutants ($PM_{2.5}$, O_3, SO_2, and NO_2) and basic meteorological parameters (wind speed, relative humidity, temperature, net radiation) during the entire measurement campaign. The probability density functions and the corresponding statistical parameters also were given in Figure 2. The mean values for N_{13-25}, N_{25-100}, and $N_{100-800}$ were 2514.0 cm^{-3}, 10768.7 cm^{-3}, and 3258.4 cm^{-3}, respectively. Aitken mode particles, accounting for 65.1% of total PNCs, were significantly higher than the other modes, and the differences

Atmospheric
Chemistry
and Physics
Discussions
Open Access
EGU

were much larger than the results at European cities (Cusack et al., 2013; Leoni et al., 2018), urban

Beijing (Wu et al., 2008) and North China Plain (Shen et al., 2011), which may be related with the fact

that the particles in 3-12 nm and 800-1000 nm were not covered in nucleation and accumulation mode

for our measurement campaign. The nucleation mode particles also can grow to Aitken mode by

5   coagulation and hygroscopicity when they were transported from the primary emissions at the ground

surface to the sampling location due to the much higher sampling height compared to the other studies.

The mean $PM_{2.5}$ and O_3, SO_2, NO_2 concentrations were 49.9 μg m^{-3}, 44.8 μg m^{-3}, 22.7 μg m^{-3} and 57.5

μg m^{-3} during 2014-2019, and mean values of wind speed, temperature, relative humidity, and net

radiation were 1.6 m s^{-1}, 10.9 ℃, and 44.6%, and 44.4 W m^{-2}, respectively.

10

Until now, numerous measurements of sub-micron PNSDs have been carried out at a variety of

locations to examine their variations and key influencing factors. Table 1 summarizes experimentally

determined particle number concentrations in the troposphere for the measurement campaigns

conducted longer than 1 year across the globe. The mean number concentrations in the three modes

15 were much lower than that in urban Beijing (Wang et al., 2013), and significantly higher than that at a

remote background station, Mt. Waliguan, one of global GAW sites in China (Kivekas et al., 2009). The

sub-micron particle number concentration was much lower compared to the most polluted cities in

India, such as Delhi (Gani et al., 2020) and Kanpur (Kanawade et al., 2014), especially Aitken and

accumulation modes. Number of the particles in Aitken and accumulation modes at Asian cities were

20 even higher than that at the urban site in Europe and North America, which may be largely related to

poor visibility at Asian cities according to Mie scattering theory. For nucleation mode, the situation is

opposite, which may be because newly formed particles rapidly scavenged by coagulation with a

mount of the larger particles at highly polluted cities (von Bismarck-Osten et al., 2013; Wang et al.,

2011).

25

3.2 Trends of PNCs, criteria air pollutants, and meteorological parameters

Besides primary emissions from human activities at urban areas, particle number concentration was

easily affected by secondarily new-formed particles, which was closely related to meteorological

conditions such as temperature, relative humidity and new radiation (Zhao et al., 2015a). Figure 3

30 shows inter-annual variations of monthly averaged particle numbers, criteria air pollutants and wind

speed during 2012-2019, and normalizes the time series data (N_{13-25}, N_{25-100}, $N_{100-800}$, PM$_{2.5}$, O$_3$, SO$_2$, NO$_2$, and wind speed) to fix values to equal 100 at the beginning of September 2012. The particle number in the three size ranges declined largely during 2012-2015 (Period I), and summer N_{13-25} decreased by around 75% in 2015 compared to that in 2013, while that in winter less varied during

5　Period I. The N_{25-100} and $N_{100-800}$ reduced more in winter than that in summer due to emission control impacts. The number in nucleation mode particles (N_{13-25}) increased significantly during 2016-2019 (Period II), which was consistent with O$_3$ while showed the opposite trend with declining PM$_{2.5}$ during Period II. The strongly declining aerosol radiative effect due to the strict air pollution controls resulted in an unprecedented rapid increasing trend in surface solar radiation over China during 2014-2019 (Shi

10　et al., 2021), which maybe promote formation of secondary air pollutants.

The particle number in the Aitken and accumulation modes (N_{25-100}, $N_{100-800}$) firstly increased during 2016-2017 and then decreased from 2018 to 2019, and their variations were consistent with the primary emitted pollutants (SO$_2$, NO$_2$), indicating that N_{25-100} and $N_{100-800}$ variations during 2016-2018 were

15　mainly modulated by primary emissions. Sun et al. (2020) analyzed the long-term trends of particle number concentrations at 16 observational sites in Germany from 2009 to 2018, and number concentrations of particles in the three modes were found to be significant decreasing trends in response to emission mitigation policies. The contrasting response of nucleation mode particle to mitigation policies between China and Germany may be related to the fact that more reduction of

20　coagulation sink due to the ever strictest Clean Air Action in China, and thus NPF event easily occurred due to less coagulation scavenging effects (Gani et al., 2020). The variation in wind speed was not significant during the entire measurement campaign.

In view of the contrasting PNC trends between Periods I and II, the below analyses compared mean

25　diurnal and annual variations of particle number in the three size bins (N_{13-25}, N_{25-100}, and $N_{100-800}$), PM$_{2.5}$ and O$_3$ as wind directions before and after January 2016 (Figures 4, S1-S4). The most obvious increase in N_{13-25} was during 12:00-16:00 in summer months after January 2016 compared to before January 2016, and the largest increase corresponded to easterly, southerly and southwesterly winds, especially for the annual cycles with the more significantly increased N_{13-25} for southeasterly winds.

30　The large CPF values of N_{13-25} mainly corresponded to southerly winds (Figure 5), which can support

the above results. N_{25-100} difference between the two periods (2012-2015 vs. 2016-2019) was much less

significant than N_{13-25}, and the most obvious N_{25-100} increase occurred in morning and evening rush

hours for northeasterly winds (Figure S1), which could be supported by the results of polar plots

(Figure 5). Figure 6 illustrated mean particle number size distributions by varying wind directions, and

5   number in Aiken mode particles for north northeasterly winds ($0°$ - $45°$) was largely higher than that for

the other wind directions. The emissions from jammed traffic and winter domestic heating with

traditional stoves at Keji Street, about 500 m away from the sampling site, could be transported to the

station as northeasterly winds. In addition, the larger increase in N_{25-100} at 13 p.m. for easterly, southerly

and southwesterly winds was consistent with N_{13-25} possibly due to new-formed particle growth

10   impacts.

The $N_{100-800}$ and $PM_{2.5}$ trends from Period I to II in diurnal and annual cycles were opposite to N_{13-25}

with the significant reduction at noon in summer months for southerly winds (Figures 5, S2 and S3),

which was mainly affected by Clean Air Action (Li et al., 2021). Gani et al. (2020) studied particle

15   number concentrations and size distributions in a polluted megacities of Delhi in India, and pointed out

that strategies that only target accumulation mode particles (which constitute much of the fine $PM_{2.5}$

mass) may even lead to an increase in the UFP concentrations as the coagulation sink decreases.

Furthermore, O_3 increased more significantly in the afternoon in summer months after than before

January 2016, and wind directions for the largest increased O_3 concentrations were consistent with

20   nucleation mode particles (Figure S4), which further confirmed that the increased N_{13-25} from Period I

to II was induced by more frequent nucleation events. Compared with before January 2016, the more

favorable meteorological conditions after January 2016 such as the much drier air (Figure S5), higher

ambient temperature (Figure S5) and stronger solar radiation (Figure S6) for southerly winds also

helped to form new particles, which could be supported by our previous work in the same site (Zhao et

25   al., 2015a).

3.3 Typical particle number size distributions influenced by varying factors

Besides chemical composition of airborne particles, the information derived from particle number size

distributions (PNSDs) is beginning to play an important role in source apportionment studies (Vu et al.,

30   2015) due to the obvious difference of diameters for the particles from varying sources. The hourly

average PNSDs during the entire measurement campaign were classified into six clusters by K-means clustering technique, and mean PNSD for each typical type was showed in Figure 7. As showed in Figure 7, the shape and mode diameter of PNSDs were largely different among the Clusters. Mode diameters varied from ~ 20 nm for Cluster B to 70 nm for Cluster F, and more than a quarter of PNSDs

5   was sorted into Cluster A with mode diameter of ~ 55 nm, while Cluster B less occurred with mode diameter of ~ 20 nm. The sources and key factors influencing each cluster of PNSD can be better determined by averagely annual and diurnal variations of occurrence frequencies, and the corresponding air pollutants and meteorological parameters for the Clusters (Figure 8, Tables 2 and 3).

10   About 70% of Clusters A and F is in the cold seasons (October-December, and January-March) with the almost opposite diurnal pattern between the two Clusters (Figure 8). Clusters A and F had the highest number concentrations of accumulation mode particles ($N_{100-800}$) and mass concentrations of particulate matter ($PM_{2.5}$, PM_{10}) and gaseous pollutants (SO_2, NO_2, CO), while the lowest particle number in nucleation mode (N_{13-25}) and O_3 mass concentrations among the clusters (Table 2), suggesting that the

15   two polluted clusters may be mainly impacted by primary emissions from human activities, and was defined and abbreviated as "Pollut_C" in the below analyses. That also can be confirmed by larger geometric median diameters for the three modes (GMD_{nuc}, GMD_{Ait}, and GMD_{acc}) than that for the other clusters, and the high particle number concentrations in morning and evening rush hours (Figure S7). Compared with other clusters, the weaker winds and net radiation, lower ambient temperature, and

20   higher relative humidity indicated that the severe air pollution for Clusters A and F was significantly affected by stable air and poor diffusion conditions. Furthermore, as illustrated in Figure 9, Cluster F (A) accounted for more than 40% (60%) of all clusters during five hours after occurrence of Cluster A (F), and the more frequently synchronous occurrence between Clusters A and F maybe related to the pollution process from "light-severe-light" episodes. From the perspectives of inter-annual variations in

25   occurrence frequency, the Pollut_C increasingly less occurred from 2014 to 2019 possibly due to implementation of Clean Air Action (Figure 8A), which will be analyzed in detail in the following section.

The Clusters B and E mainly appeared in the daytime in the warmer months, and occurrence frequency

30   had a sharp peak in the afternoon (Figures 8B and 8C), and the peak for Cluster E lagged around two

hours than that for Cluster B. The frequency of Cluster E during two hours after occurrence of Cluster
B was larger than 80%, and mode diameter of Cluster E (~ 30 nm) was only larger than that of Cluster
B (~ 20 nm), and thus it was inferred that Cluster B represented secondarily new particle formation
(NPF) event impacts, while Cluster E was influenced by subsequently new particle growth events. The

5   inference could be confirmed by the highest particle number in nucleation mode and O_3 mass
concentration among the clusters (Table 2). The sharply increased nucleation mode particles at 9:00
was followed by a subsequent growth to accumulation mode indicated by the typical "banana-shaped"
temporal development of the number size distribution (Figure S7, Boy and Kulmala, 2002), which also
supported the above inference. In addition, the less coagulation sink such as low number concentrations

10   of particles in accumulation mode, and low $PM_{2.5}$ and PM_{10} mass induced by higher wind speed helped
to form secondarily new particles (Tables 2 and 3). The more recent study of Gani et al. (2020)
investigated particle number concentrations and size distribution in a polluted megacity: the Delhi, and
found that reduction in mass concentration in the highly polluted megacity may not produce a
proportional reduction in PNCs, and may even lead to an increase in the UFP concentrations as the

15   coagulation sink decreases. The mean AOD of 0.39 for Cluster B was significantly lower than that for
the other clusters (Table 2), which resulted in the higher atmospheric transparency and thus stronger net
radiation (223.55 W m^{-2}) and higher ambient temperature (20.77 °C). The drier air was conducive to
detecting NPF events and newly formed particles grown hard by hygroscopic growth under low RH
environments. The occurrence frequency for the two clusters first reduced from 2013 to 2015 and then

20   increased until 2019, which contrasted with the "Pollut_C" during the campaign. Clusters B and E were
abbreviated as "NPF_C" for the following analyses.

The mean PNSD for Cluster C was much wider and more flat than that for the other clusters and thus it
was hard to determine the mode diameter, especially for the PNSDs from dawn to noon (Figures 7 and

25   S7). The number of particles in nucleation mode (N_{13-25}) was only lower than NPF_C while that in
accumulation mode ($N_{100-800}$) was only lower than Pollut_C. The cluster was more easily occurred in
the morning in the warm months, which was consistent with most of the clusters except the polluted
Clusters A and F. Additionally, except for Cluster F, the occurrence frequency of the other clusters was
comparable and ranged from about 15% to 28% during 1-12 hours after Cluster C. The frequency of

30   Cluster C also less varied during 1-12 hours after Clusters A, D, E and F (Figure 9). Combined the

above fact with the modest concentrations of particle number in the three modes, criteria air pollutants and meteorological parameters, it was inferred Cluster C representing urban background PNSD, and thus it was defined as "UB_C" in the following analyses. Cluster D more frequently occurred in the morning and evening rush hours in the warm seasons (Figure 8), and the correspondingly mean particle

5   number in Aitken mode (N_{25-100}) was the second highest ever-just behind Cluster A, which may be impacted by motor vehicle emissions from the nearby roads. The mode diameter of ~ 40 nm was only larger than NPF_C (Clusters A and E), and it appeared frequently after Cluster E with the high concentration of particles in Aitken mode in the afternoon (Figure S7) possibly due to new particle growth impacts. Therefore, Cluster D was jointly influenced by motor vehicle emissions and NPF

10   events, and was defined as "VE_NPF_C" in the following section.

From the perspectives of the variation in mode diameter among the clusters (Figure 7) and the variation in frequency during 1-12 hours after each cluster (Figure 9), the NPF_C was closely followed by Pollut_C during the measurement campaign, and the clusters can be ranked by temporal order as

15   "B→E→D→A→F". Therefore, NPF events significantly contributed to haze episodes in the subsequent 1–2 days, which may be increasingly obvious mainly due to considerably decreased emissions of primary particles during recent years in response to Clean Air Action. Guo et al. (2014) first reported that atmospheric NPF tends to precede winter haze episodes in Beijing, and then the latest study of Kulmala et al. (2021) investigate how NPF and subsequent particle growth affect the initial

20   steps of haze formation in Beijing. Their findings showed that reducing the subsequent growth rate of freshly formed particles by a factor of 3–5 would delay the buildup of haze episodes by 1–3 days.

3.4 Impact of Clean Air Action on PNC variations

The response of $PM_{2.5}$ mass to Clean Air Action has been evaluated in many previous studies, and

25    $PM_{2.5}$ was found to be decreased by 30%-50% across China during 2013-2018 due to the implementation of emission control policies (Zhai et al., 2019). The impact of the policies on particle number may be more complex as compared to PM mass since more fine particles cannot rapidly grow by coagulation with the reduced coarse particles (Gani et al., 2020). However, the response of PNCs to the restricted emissions was only analyzed by some short-term measurements during some important

30   and international meetings and activities such as the summer Olympic Games in 2008 and the

Asia-Pacific Economic Cooperation (APEC) in 2014 and China's V-Day parade in 2015 (Chen et al., 2015; Shen et al., 2016; Wang et al., 2013). The Long-term *in-situ* measurements of PNSDs and mass concentrations of the criteria air pollutants was essential to understand the emission control impacts and to reveal the mechanism. Figures 10, S8 and S9 show trends of daily mean particle number in the three

5   modes as wind directions for each cluster based on 7.5 years measurement. The number of particles in nucleation mode (N_{13-25}) first decreased from 2012 to 2015, and then increased rapidly after 2016. The N_{13-25} changing trend for NPF_C (Clusters B and E) was more significant as compared with that for the other clusters, especially for southeasterly winds. The specific winds corresponded to more $PM_{2.5}$ reduction on summer afternoon after than before 2016 due to impact of emission mitigation policies

10   (Figure S3), and thus NPF events, represented by NPF_C, were easily detected by chemical reactions due to reduced coagulation sink. The more solar radiation reached near-surface air as a result of reduced $PM_{2.5}$ mass (Shi et al., 2021), and thus ambient temperature increased and relative humidity declined (Figures S5 and S6), which also favored occurrence of NPF events (Zhao et al., 2015a).

15   At our sampling site, N_{25-100} was easily influenced by growth of newly formed particles and primary emissions from human activities. The N_{25-100} trends was similar with N_{13-25} for Clusters B, D and E, and the increasing trends also were more significant after 2016 for southwesterly winds (Figure S8), which represented NPF impacts. Dependence of N_{25-100} on wind directions was not obvious for Clusters A, C and F, and thus the trends may be related to variations in primary emissions. Unlike nucleation and

20   Aitken modes, particle number in accumulation mode ($N_{100-800}$) less depended on wind directions. Furthermore, $N_{100-800}$ was the lowest and less varied for NPF_C, while that for Clusters A, C and D had similar trend with N_{25-100}, and that for Cluster F, the most polluted cluster, was downward trend during the campaign due to implementation of the strictest ever Clean Air Action. Therefore, the response of particle number to air pollution control may be largely different for each size fraction, which may be

25   closely related to the variations in coagulation sink and meteorological conditions induced by reduced primary emissions. That will be discussed in detail in the following section.

To better evaluate variations in particle number concentrations and emission control impacts, Figures 11, S10 and S11 show variations of contributions of each cluster to monthly averaged PNCs in 13-25

30   nm, 25-100 nm and 100-800 nm during the campaign, respectively. Pollut_C (Clusters A and F)

Atmospheric
Chemistry
and Physics
Discussions

Open Access

EGU

dominated the winter PNCs in different size bins before 2016, and their occurrence was less and less

frequent after 2016, especially for the most polluted Cluster F, which was largely dominated by

reduction in primary emissions. Contrasting to Pollut_C, as a main cluster representing NPF events, the

contribution of Cluster B to summer N_{13-25} decreased from 50% to about 10% during 2013 to 2015, and

5   then increased to reach around 60% in 2019. For Cluster C representing urban background, its

frequency less varied during the entire measurement campaign. The particle number was dominated by

primary emissions before 2016, and thereafter that was controlled by NPF events, which was partly due

to emission control. In response to air pollution control, the reduction in coarse particles could promote

secondary new particle formation by reduced coagulation sink (Gani et al., 2020). NPF events were

10   largely dependent on PM mass concentrations mainly contributed by coarse aerosol particles.

Accumulation mode particle number concentrations in cities of developing countries are generally

higher than that in many western cities (Gani et al., 2020; Wu et al., 2008), and thus the response of

NPF events to emission control may be largely different between the cities of developed and

developing countries. For example, Sun et al. (2020) found that coincidently downward trends of

15   particle number and black carbon mass concentrations at 16 observational sites in Germany from 2009

to 2018 due to reduced anthropogenic emissions. Gani et al. (2020) pointed out that strategies that only

target accumulation mode particles in a polluted megacity in India may even lead to an increase in the

UFP concentrations as the coagulation sink decreases. Shen et al. (2016) also found that PM_1 mass

concentration was significantly reduced while NPF event frequency was much higher during short-term

20   emission control period.

We also quantitatively evaluated the changing trends of particle number in the three modes by

Theil-Sen regression. In view of the contrasting trends, the observation period was divided into two

sub-periods, i.e., before and after January 2016. Figures 12 and 13 illustrated seasonal and diurnal

25   variations of trends of PNCs for each cluster during each sub-period. For Period I (2012-2015), PNCs

in the three size bins exhibited downward trends for all clusters, especially in spring. The annual

relative slopes of spring PNCs varied from -54.7% for Cluster F to -17.2% for Cluster B, -42.6% for

Cluster A to -14.1% for Cluster B, and -40.7% for Cluster A to -17.5% for Cluster B per year for 13-25,

25-100, and 100-800 nm size ranges (Figure 12). The PNCs for Pollut_C (Clusters A and F) decreased

30   by about 40% in the morning and evening rush hours, which was much higher than that in the other

hours of day. Therefore, the more reduction in PNCs for Pollut_C may be closely related to emission

control policies. The much larger PNC reduction in this study than that in Germany may be due to

implementation of the stricter ever emission mitigation policies in Chinese cities (Sun et al., 2020).

Contrary to Period I, the UFPs number was increased and the amplitude was greater during Period II

5   (2016-2019). The annual relative slopes of N_{13-25} varied between 5.1% (fall) and 314.4% (winter), 8.0

(fall) and 135.5% (spring), 11.3% (fall) and 184.3% (winter), -4.5 (fall) and 59.1% (summer), 6.3%

(fall) and 30.3% (spring), and 3.6% (fall) and 15.7% (spring) for Clusters A-F. The maximum increase

of N_{13-25} was in the spring afternoon for NPF_C, which may be governed by NPF events due to reduced

coagulation sink corresponding to low $N_{100-800}$. The winter N_{13-25} was increased significantly for Cluster

10   A during Period II, especially in the morning and evening rush hours, suggesting the impact of primary

emissions from motor vehicles. The annual slope of $N_{100-800}$ less varied as compared to that of ultrafine

particles in seasonal and diurnal cycles.

3.5 Role of meteorology and air masses

15   NPF events predominantly occurred under dry and sunny weather conditions (Birmili and

Wiedensohler, 2000). Figures 14 and 15 show the diurnal and inter-annual variations in meteorological

parameters such as net radiation, temperature, relative humidity, and wind speed and direction for each

cluster during the campaign to better understand response of PNCs to meteorology. The peak of net

radiation and N_{13-25} coincided at noon for NPF_C, and their peaks were largely higher than that for the

20   other clusters (Figure 14). The increased daylight net radiation for Cluster B also could partly explain

the higher N_{13-25} induced by the more frequent NPF events after 2016, especially in spring (Figures 15

and S12). The higher ambient temperature and lower relative humidity at noon and the larger daily

ranges for NPF_C also indicated that dry and hot air in sunny day was conducive to form new particles.

In addition, NPF events corresponding to large southeasterly winds may be because accumulation

25   mode particles were dispersed and diluted by strong winds and thus coagulation sink decreased, which

can be supported by the above results. According to empirically based mathematical function between

number concentrations of fine particles (FP, diameter <2.5 μm) and meteorological variables, Hussein

et al. (2006) found that the predicted number concentrations of accumulation mode particles follow this

relationship more closely than those of UFP's due to the origin and type of aerosol particles in the

30   accumulation mode size range, being mainly regional and long-range transported. The main limitation

of the mathematical function in their study was during NPF events, indicating that particles in

nucleation and accumulation modes were differently dependent on meteorological variables.

A general finding was that changes in aerosol were related to air mass changes (Birmili et al., 2001),

5 and dust aerosols from Gobi Deserts at Hexi Corridor could be transported to Lanzhou and affected

urban PM pollution (Zhao et al., 2015b). Figure 16 illustrates gridded back trajectory frequencies with

hexagonal binning for each cluster to explore the impacts of air mass on variations of particle number.

The huge discrepancy of back trajectory frequencies among the six clusters suggested that the air mass

history has a significant impact on urban particle number concentrations and size distributions. For

10 example, back trajectories were mainly from the adjacent regions of urban Lanzhou and less affected

by long-range transport for NPF_C, and the thus particles were not easily grown by coagulation during

transport processes, which was conducive to occurrence of NPF events. In urban Beijing, Wang et al.

(2013) also indicated that mean total PNCs from north directions were higher than the air masses that

came from other directions, while more volume concentrations were observed for the air masses from

15 the southwest and the south. Therefore, particle number size distributions in urban Lanzhou were partly

affected by air mass conditions.

4 Summary and conclusions

The first *in-situ* observations of particle number size distributions (PNSDs) in the size range of 13-800

20 nm were conducted from 2012 to 2019 in urban Lanzhou, a typical valley city in west China.

Meanwhile, the mass concentrations of the criteria air pollutants ($PM_{2.5}$, PM_{10}, O_3, SO_2, NO_2, and CO),

AOD and meteorological variables (temperature, relative humidity, wind speed and direction and net

radiation) also were measured during the campaign. The customized Sen-Theil trend estimator and

K-means clustering technique were used to explore the trends of PNCs and the criteria air pollutants,

25 and to reveal the contributions of variations in primary emissions due to Clean Air Action and

secondary formation to PNCs. Some novel findings were obtained as follows.

The mean values for particle number in nucleation (N_{13-25}), Aitken (N_{25-100}) and accumulation modes

($N_{100-800}$) were respectively 2514.0 cm^{-3}, 10768.7 cm^{-3}, and 3258.4 cm^{-3}, and N_{25-100} accounted for about

30 65.1% of total PNCs during the campaign. The particle number in the three modes declined largely

during 2012-2015 such as summer N_{13-25} decreased by around 75% in 2015 compared to that in 2013. However, N_{13-25} increased significantly during 2016-2019, which was consistent with O_3 while showed the opposite trend with declining $PM_{2.5}$ during the period. The most obvious increase in N_{13-25} was during 12:00-16:00 in summer months, and the largest increase corresponded to easterly, southerly and

5 southeasterly winds. The N_{25-100} and $N_{100-800}$ firstly increased during 2016-2017 and then decreased until 2019, and their variations were consistent with the primary emitted pollutants (SO_2, NO_2). N_{25-100} difference between the two periods (2012-2015 vs. 2016-2019) was much less significant than N_{13-25}, and the most obvious N_{25-100} increase occurred in morning and evening rush hours for northeasterly winds. In diurnal and annual cycles, the $N_{100-800}$ and $PM_{2.5}$ trends for the two periods were opposite to

10 N_{13-25} with the significant reduction at noon in summer months for southerly winds, and thus decreased coagulation sink was conducive to occurrence of NPF events.

K-means clustering technique was used to classify the hourly average PNSDs into six clusters during the measurement campaign. The shape and mode diameter of PNSDs were largely different among the

15 clusters with varying mode diameters from ~ 20 nm to 70 nm. According to the annual and diurnal variations of occurrence frequency, PNSD, the corresponding air pollutants and meteorological parameters, the sources and key influencing factors were determined for each cluster. The two most polluted clusters (A and F), Pollut_C, were mainly affected by the primary emissions from human activities and poor diffusion conditions. Cluster B was followed by Cluster E, and N_{13-25} had a sharp

20 peak in the afternoon in the warm months, and thus the two clusters represented new particle formation and growth event impacts. Cluster C suggested urban background PNSD, while Cluster D was jointly affected by motor vehicle emissions and NPF events. The response of particle number to air pollution control was largely different for each size fraction, which may be closely related to the variations in coagulation sink and meteorological conditions induced by reduced primary emissions. Based on trends

25 of daily mean particle number in the three modes as wind directions for each cluster, the contributions of primary emissions and secondary formation to PNCs were evaluated in this study. The southeasterly winds corresponded to more $PM_{2.5}$ reduction on summer afternoon in response to emission control policies and thus more solar radiation reached ground surface, which promoted NPF occurrence due to decreased coagulation sink. The polluted clusters governed the winter PNCs before 2016, and their

30 occurrence was less and less frequent after 2016, which was largely dominated by reduction in primary

emissions. However, the contribution of NPF events to summer N_{13-25} decreased from 50% to about 10% during 2013 to 2015, and then increased to reach around 60% in 2019.

5   Theil-Sen regression was used to quantitatively evaluate the changing trends of size-resolved PNCs, and they exhibited downward trends for all clusters during 2012-2015, especially in spring. The annual relative slopes of spring PNCs varied from -54.7% for Cluster F to -17.2% for Cluster B, -42.6% for Cluster A to -14.1% for Cluster B, and -40.7% for Cluster A to -17.5% for Cluster B per year for 13-25, 25-100, and 100-800 nm size ranges. The UFPs number was increased and the amplitude was greater during 2016-2019. The annual relative slopes of N_{13-25} varied between 5.1% (fall) and 314.4% (winter),

10   8.0 (fall) and 135.5% (spring), 11.3% (fall) and 184.3% (winter), -4.5 (fall) and 59.1% (summer), 6.3% (fall) and 30.3% (spring), and 3.6% (fall) and 15.7% (spring) for Clusters A-F. The increased daytime net radiation, higher ambient temperature and lower relative humidity at noon for NPF events also could partly explain the higher N_{13-25} induced by the more frequent nucleation events after 2016, especially in spring. The air mass history had a significant impact on urban PNSDs. The back

15   trajectories were mainly from the adjacent regions of urban Lanzhou and less affected by long-range transport for NPF events, and the thus particles were not easily grown by coagulation during transport processes, which was helpful for occurrence of NPF events. In this study, the measurement campaign was conducted at a Chinese cities in west China, but the similar PNCs trends and influencing factors should be expected in other Chinese cities. In future work, we will established the PNSD observation

20   network in some megacities to better evaluate the response of PNCs to emission mitigation policies in China.

Author contributions. Suping Zhao and Ye Yu designed the study. Suping Zhao analyzed the data with help from Ye Yu and Dahe Qin. Daiying Yin and Longxiang Dong collected and analyzed particle number size distributions

25   and meteorology data during the campaign. Jianglin Li conducted the field experiment.

Competing interests. The authors declare that they have no conflict of interest.

References

Andreae, M. O., and Rosenfeld, D.: Aerosol-cloud-precipitation interactions. Part 1. The nature and

sources of cloud-active aerosols, Earth-Science Reviews, 89(1-2), 13-41, 2008.

Asmi, A., Wiedensohler, A., Laj, P., Fjaeraa, A.-M., Sellegri, K., Birmili, W., Weingartner, E.,

Baltensperger, U., Zdimal, V., Zikova, N., Putaud, J.-P., Marinoni, A., Tunved, P., Hansson, H.-C.,

Fiebig, M., Kivekas, N., Lihavainen, H., Asmi, E., Ulevicius, V., Aalto, P. P., Swietlicki, E., Kristensson,

A., Mihalopoulos, N., Kalivitis, N., Kalapov, I., Kiss, G., de Leeuw, G., Henzing, B., Harrison, R. M.,

Beddows, D., O'Dowd, C., Jennings, S. G., Flentje, H., Weinhold, K., Meinhardt, F., Ries, L., and

Kulmala, M.: Number size distributions and seasonality of submicron particles in Europe 2008–2009,

Atmospheric Chemistry and Physics, 11, 5505–5538, 2011.

Asmi, A., Collaud Coen, M., Ogren, J. A., Andrews, E., Sheridan, P., Jefferson, A., Weingartner, E.,

Baltensperger, U., Bukowiecki, N., Lihavainen, H., Kivekäs, N., Asmi, E., Aalto, P. P., Kulmala, M.,

Wiedensohler, A., Birmili, W., Hamed, A., O'Dowd, C., G Jennings, S., Weller, R., Flentje, H., Fjaeraa,

A. M., Fiebig, M., Myhre, C. L., Hallar, A. G., Swietlicki, E., Kristensson, A., and Laj, P.: Aerosol

decadal trends – Part 2: In-situ aerosol particle number concentrations at GAW and ACTRIS stations,

Atmospheric Chemistry and Physics, 13, 895–916, https://doi.org/10.5194/acp-13-895-2013, 2013.

Birmili, W., and Wiedensohler, A.: New particle formation in the continental boundary layer:

Meteorological and gas phase parameter influence, Geophysical Research Letters, 27, 3325-3328,

2000.

Birmili, W., Wiedensohler, A., Heintzenberg, J., and Lehmann, K.: Atmospheric particle number size

distribution in central Europe: Statistical relations to air mass and meteorology, Journal of Geophysical

Research, 32, 5–18, 2001.

Birmili, W., Heinke, K., Pitz, M., Matschullat, J., Wiedensohler, A., Cyrys, J., Wichmann, H.-E., and

Peters, A.: Particle number size distributions in urban air before and after volatilization, Atmospheric

Chemistry and Physics, 10, 4643–4660, 2010.

Birmili, W., Weinhold, K., Rasch, F., Sonntag, A., Sun, J., Merkel, M., Wiedensohler, A., Bastian, S.,

Schladitz, A., Löschau, G., Cyrys, J., Pitz, M., Gu, J. W., Kusch, T., Flentje, H., Quass, U., Kaminski,

H., Kuhlbusch, T. A. J., Meinhardt, F., Schwerin, A., Bath, O., Ries, L., Gerwig, H., Wirtz, K., and

Fiebig M.: Long-term observations of tropospheric particle number size distributions and equivalent

black carbon mass concentrations in the German Ultrafine Aerosol Network (GUAN), Earth System

Science Data, 8, 355–382, 2016.

5   Bodhaine, B. A.: Aerosol measurements at four background sites, Journal of Geophysical Research,

88(C15), 10753–10768, doi:10.1029/JC088iC15p10753, 1983.

Boy, M. and Kulmala, M.: Nucleation events in the continental boundary layer: influence of physical

and meteorological parameters, Atmospheric Chemistry and Physics, 2, 1–16, 2002.

Chen, C., Sun, Y. L., Xu, W. Q., Du, W., Zhou, L. B., Han, T. T., Wang, Q. Q., Fu, P. Q., Wang, Z. F.,

10   Gao, Z. Q., Zhang, Q., and Worsnop, D. R.: Characteristics and sources of submicron aerosols above

the urban canopy (260 m) in Beijing, China during 2014 APEC summit, Atmospheric Chemistry and

Physics, 15, 12879–12895, 2015.

Chen, C. H., Huang, J. G., Ren, Z. H., and Peng, X. A.: Meteorological conditions of photochemical

smog pollution during summer in Xigu industrial area, Acta Scientiae Circumstantiae (in Chinese), 6(3),

15   334–342, 1986.

Chu, P. C., Chen, Y. C., Lu, S. H., Li, Z. C., and Lu Y. Q.: Particulate air pollution in Lanzhou China,

Environment International, 34, 698–713, 2008.

Cusack, M., Perez, N., Pey, J., Alastuey, A., and Querol, X.: Source apportionment of fine PM and

sub-micron particle number concentrations at a regional background site in the western Mediterranean:

20   a 2.5 year study, Atmospheric Chemistry and Physics, 13, 5173–5187, 2013.

Dal Maso, M., Kulmala, M., Riipinen, I., Wagner, R., Hussein, T., Aalto, P. P., and Lehtinen, K. E. J.:

Formation and growth of fresh atmospheric aerosols: eight years of aerosol size distribution data from

SMEAR II, Hyytiala, Finland, Boreal Environment Research, 10, 323–336, 2005.

Dal Maso, M., Hyvärinen, A., Komppula, M., Tunved, P., Kerminen, V.-M., Lihavainen, H., Öviisanen,

25   Y., Hansson, H.-C., and Kulmala, M.: Annual and interannual variation in boreal forest aerosol particle

number and volume concentration and their connection to particle formation, Tellus B: Chemical and

Physical Meteorology, 60(4), 495–508, 2008.

Dinoi, A., Weinhold, K., Wiedensohler, A., and Contini, D.: Study of new particle formation events in

southern Italy, Atmospheric Environment, 244, 117920, 2021.

30   Gani, S., Bhandari, S., Patel, K., Seraj, S., Soni, P., Arub, Z., Habib, G., Hildebrandt Ruiz, L., and Apte,

J. S.: Particle number concentrations and size distribution in a polluted megacity: the Delhi Aerosol

Supersite study, Atmospheric Chemistry and Physics, 20, 8533–8549, 2020.

Gao, Y., Zhang, M., Liu, Z., Wang, L., Wang, P., Xia, X., Tao, M., and Zhu, L.: Modeling the feedback

between aerosol and meteorological variables in the atmospheric boundary layer during a severe

5   fog-haze event over the North China Plain, Atmospheric Chemistry and Physics, 15(8), 4279–4295.

https://doi.org/10.5194/acp-15-4279-2015, 2015.

Guo, S., Hu, M., Zamora, M. L., Peng, J., Shang, D., Zheng, J., Du, Z., Wu, Z., Shao, M., Zeng, L.,

Molina, M. J., and Zhang, R. Y.: Elucidating severe urban haze formation in China, Proceedings of the

National Academy of Sciences of the United States of America, 111(49), 17373-17378,

10   www.pnas.org/cgi/doi/10.1073/pnas.1419604111, 2014.

Heintzenberg, J., Birmili, W., Otto, R., Andreae, M. O., Mayer, J.-C., Chi, X., and Panov, A.: Aerosol

particle number size distributions and particulate light absorption at the ZOTTO tall tower (Siberia),

2006–2009, Atmospheric Chemistry and Physics, 11, 8703–8719, 2011.

Hu, J., Huang, L., Chen, M., Liao, H., Zhang, H., Wang, S., Zhang Q., and Ying Q.: Premature

15   mortality attributable to particulate matter in China: source contributions and responses to reductions,

Environmental Science and Technology, 51(17), 9950-9959, 2017.

Hussein, T., Puustinen, A., Aalto, P. P., Mäkelä, J. M., Hämeri, K., and Kulmala, M.: Urban aerosol

number size distributions, Atmospheric Chemistry and Physics, 4, 391–411, 2004.

Hussein, T., Karppinen, A., Kukkonen, J., Harkonen, J., Aalto, P. P., Hämeri, K., Kerminen, V.-M., and

20   Kulmala, M.: Meteorological dependence of size-fractioned number concentrations of urban aerosol

particles, Atmospheric Environment, 40, 1427–1440, 2006.

Kanawade, V. P., Tripathi, S. N., Bhattu, D., and Shamjad, P. M.: Sub-micron particle number size

distributions characteristics at an urban location, Kanpur, in the Indo-Gangetic Plain, Atmospheric

Research, 147-148, 121-132, 2014.

25   Kivekas, N., Sun, J., Zhan, M., Kerminen, V.-M., Hyvarinen, A., Komppula, M., Viisanen, Y., Hong, N.,

Zhang, Y., Kulmala, M., Zhang, X.-C., Geer. D., and Lihavainen, H.: Long term particle size

distribution measurements at Mount Waliguan, a high-altitude site in inland China, Atmospheric

Chemistry and Physics, 9, 5461–5474, 2009.

Krecl, P., Johansson, C., Targino, A. C., Strom, J., and Burman, L.: Trends in black carbon and

30   size-resolved particle number concentrations and vehicle emission factors under real-world conditions,

Atmospheric Environment, 165, 155–168, 2017.

Kulmala, M.: How particles nucleate and grow, Science, 302, 1000–1001, 2003.

Kulmala, M., Vehkamäki, H., Petäjä, T., Dal Maso, M., Lauri, A., Kerminen, V. M., Birmili, W., and
McMurry, P. H.: Formation and growth rates of ultrafine atmospheric particles: a review of

5   observations. Journal of Aerosol Science, 35, 143–176, 2004.

Kulmala, M., Dada, L., Daellenbach, K. R., Yan, C., Stolzenburg, D., Kontkanen, J., Ezhova, E.,
Hakala, S., Tuovinen, S., Kokkonen, T. V., Kurppa, M., Cai, R. L., Zhou, Y., Yin, R., Baalbaki, R.,
Chan, T., Chu, B., Deng, C., Fu, Y., Ge, M. F., He, H., Heikkinen, L., Junninen, H., Liu, Y., Lu, Y., Nie,
W., Rusanen, A., Vakkari, V., Wang, Y., Yang, G., Yao, L., Zheng, J., Kujansuu, J., Kangasluoma, J.,

10   Petaja, T., Paasonen, P., Jarvi, L., Worsnop, D., Ding, A. J., Liu, Y., Wang, L., Jiang, J. K., Bianchi, F.,
and Kerminen, V.-M.: Is reducing new particle formation a plausible solution to mitigate particulate air
pollution in Beijing and other Chinese megacities? Faraday Discussions, 226, 334-347, DOI:
10.1039/d0fd00078g, 2021.

Lelieveld, J., Evans, J. S., Fnais, M., Giannadaki, D. and Pozzer, A.: The contribution of outdoor air

15   pollution sources to premature mortality on a global scale, Nature, 525, 367, DOI:
10.1038/nature15371, 2015.

Leoni, C., Pokorna, P., Hovorka, J., Masiol, M., Topinka, J., Zhao, Y. J., Krumal, K., Cliff, S., Mikuska,
P., and Hopke, P. K.: Source apportionment of aerosol particles at a European air pollution hot spot
using particle number size distributions and chemical composition, Environmental Pollution, 234, 145–

20   154, 2018.

Li, J., Gao, W., Cao, L., Xiao, Y., Zhang, Y., Zhao, S., Liu, Z., Liu, Z., Tang, G., Ji, D., Hu, B., Song, T.,
He, L., Hu, M., and Wang, Y. S.: Significant changes in autumn and winter aerosol composition and
sources in Beijing from 2012 to 2018: Effects of clean air actions, Environmental Pollution, 268,
115855, 2021.

25   Li, Z., Rosenfeld, D., and Fan, J.: Aerosols and their impact on radiation, clouds, precipitation, and
severe weather events. Oxford Research Encyclopedias,
https://doi.org/10.1093/acrefore/9780199389414.013.126, 2017.

Liu, H., Pan, X. L., Wu, Y., Ji, D. S., Tian, Y., Chen, X. S., and Wang, Z. F.: Size-resolved mixing state
and optical properties of black carbon at an urban site in Beijing, Science of the Total Environment,

30   749, 141523, 2020.

Ma, N., and Birmili, W.: Estimating the contribution of photochemical particle formation to ultrafine particle number averages in an urban atmosphere, Science of the Total Environment, 512/513, 154–166, 2015.

Makela, J. M., Aalto, P., Jokinen, V., Pohja, T., Nissinen, A., Palmroth, S., Markkanen, T., Seitsonen, K.,

5   Lihavainen, H., and Kulmala, M.: Observations of ultrafine aerosol particle formation and growth in boreal forest, Geophysical Research Letters, 24, 1219–1222, 1997.

Oberdörster, G., Oberdörster, E., and Oberdörster, J.: Nanotoxicology: An emerging discipline evolving from studies of ultrafine particles, Environmental Health Perspectives, 113, 823–839, 2005.

Pandolfi, M., Querol, X., Alastuey, A., Jimenez, J. L., Jorba, O., Day, D., Ortega, A., Cubison, M. J.,

10   Comerón, A., Sicard, M., Mohr, C., Prévôt, A. S. H., Minguillón, M. C., Pey, J., Baldasano, J. M., Burkhart, J. F., Seco, R., Peñuelas, J., van Drooge, B. L., Artiñano, B., Di Marco, C., Nemitz, E., Schallhart, S., Metzger, A., Hansel, A., Lorente, J., Ng, S., Jayne, & J., and Szidat, S.: Effects of sources and meteorology on particulate matter in the Western Mediterranean Basin: An overview of the DAURE campaign, Journal of Geophysical Research: Atmospheres, 119, 4978–5010, 2014.

15   Rose, C., Collaud Coen, M., Andrews, E., Lin, Y., Bossert, I., Lund Myhre, C., et al.: Seasonality of the particle number concentration and size distribution: a global analysis retrieved from the network of Global Atmosphere Watch (GAW) near-surface observatories, Atmospheric Chemistry and Physics Discussions, https://doi.org/10.5194/acp-2020-1311, 2021.

Sabaliauskas, K., Jeong, C.-H., Yao, X., Jun, Y.-S., and Evans, G.: Cluster analysis of roadside ultrafine

20   particle size distributions, Atmospheric Environment, 70, 64–74, 2013.

Schmale, J., Henning, S., Decesari, S., Henzing, B., Keskinen, H., Sellegri, K., Ovadnevaite, J., Pöhlker, M. L., Brito, J., Bougiatioti, A., Kristensson, A., Kalivitis, N., Stavroulas, I., Carbone, S., Jefferson, A., Park, M., Schlag, P., Iwamoto, Y., Aalto, P., Äijälä, M., Bukowiecki, N., Ehn, M., Frank, G., Fröhlich, R., Frumau, A., Herrmann, E., Herrmann, H., Holzinger, R., Kos, G., Kulmala, M., Mihalopoulos, N.,

25   Nenes, A., O'Dowd, C., Petäjä, T., Picard, D., Pöhlker, C., Pöschl, U., Poulain, L., Prévôt, A. S. H., Swietlicki, E., Andreae, M. O., Artaxo, P., Wiedensohler, A., Ogren, J., Matsuki, A., Yum, S. S., Stratmann, F., Baltensperger, U., and Gysel, M.: Long-term cloud condensation nuclei number concentration, particle number size distribution and chemical composition measurements at regionally representative observatories, Atmospheric Chemistry and Physics, 18, 2853–2881,

30   https://doi.org/10.5194/acp-18-2853-2018, 2018.

Schmid, O. and Stoeger, T.: Surface area is the biologically most effective dose metric for acute nanoparticle toxicity in the lung, Journal of Aerosol Science, 99, 133–143, 2016.

Seinfeld, J. H. and Pandis, S. N.: Atmospheric chemistry and physics of air pollution, John Wiley and Sons, Inc., New York, USA, 2006.

5   Shen, X. J., Sun, J. Y., Zhang, Y. M., Wehner, B., Nowak, A., Tuch, T., Zhang, X. C., Wang, T. T., Zhou, H. G., Zhang, X. L., Dong, F., Birmili, W., and Wiedensohler, A.: First long-term study of particle number size distributions and new particle formation events of regional aerosol in the North China Plain, Atmospheric Chemistry and Physics, 11, 1565–1580, 2011.

Shen, X. J., Sun, J. Y., Zhang, X. Y., Zhang, Y. M., Zhang, L., Fan, R. X., Zhang, Z. X., Zhang, X. L.,

10   Zhou, H. G., Zhou, L. Y., Dong, F., and Shi, Q. F.: The influence of emission control on particle number size distribution and new particle formation during China's V-Day parade in 2015, Atmospheric Chemistry and Physics, 573, 409–419, 2016.

Shi, H. R., Zhang, J. Q., Zhao, B., Xia, X. A., Hu, B., Chen, H. B., Wei, J., Liu, M. Q., Bian, Y. X., Fu, D. S., Gu, Y., and Liou, K.-N.: Surface Brightening in Eastern and Central China Since the

15   Implementation of the Clean Air Action in 2013: Causes and Implications, Geophysical Research Letters, 48(3), e2020GL091105, 2021.

Stanier, C. O., Khlystov, A. Y., and Pandis, S. N.: Ambient aerosol size distributions and number concentrationsmeasured during the Pittsburgh Air Quality Study (PAQS), Atmospheric Environment, 38, 275–3284, 2004.

20   Sun, J., Birmili, W., Hermann, M., Tuch, T., Weinhold, K., Merkel, M., Rasch, F., Müller, T., Schladitz, A., Bastian, S., Löschau, G., Cyrys, J., Gu, J. W., Flentje, H., Briel, B., Asbach, C., Kaminski, H., Ries, L., Sohmer, R., Gerwig, H., Wirtz, K., Meinhardt, F., Schwerin, A., Bath, O., Ma, N., and Wiedensohler, A.: Decreasing trends of particle number and black carbon mass concentrations at 16 observational sites in Germany from 2009 to 2018. Atmospheric Chemistry and Physics, 20, 7049–7068, 2020.

25   Tunved, P., Strom, J., and Hansson, H.-C.: An investigation of processes controlling the evolution of the boundary layer aerosol size distribution properties at the Swedish background station aspvreten, Atmospheric Chemistry and Physics, 4, 2581–2592, 2004.

von Bismarck-Osten, C., Birmili, W., Ketzel, M., Massling, A., Petäjä, T., and Weber, S.: Characterization of parameters influencing the spatio-temporal variability of urban particle number size

30   distributions in four European cities, Atmospheric Environment, 77, 415-429, 2013.

Vu, T. V., Delgado-Saborit, J. M., and Harrison, R. M.: Review: Particle number size distributions from seven major sources and implications for source apportionment studies, Atmospheric Environment, 122, 114–132, 2015.

Wang, Y., Hopke, P. K., Chalupa, D. C., and Utell, M. J.: Long-term study of urban ultrafine particles
5 and other pollutants, Atmospheric Environment, 45(40), 7672-7680, 2011.

Wang, Z. B., Hu, M., Wu, Z. J., Yue, D. L., He, L. Y., Huang, X. F., Liu, X. G., and Wiedensohler, A.: Long-term measurements of particle number size distributions and the relationships with air mass history and source apportionment in the summer of Beijing, Atmospheric Chemistry and Physics, 13, 10159–10170, 2013.

10 Wehner, B., Wiedensohler, A., Tuch, T. M., Wu, Z. J., Hu, M., Slanina, J., and Kiang, C. S.: Variability of the aerosol number size distribution in Beijing, China: New particle formation, dust storms, and high continental background, Geophysical Research Letters, 31, L22108, 2004.

Wehner, B., Birmili, W., Ditas, F., Wu, Z., Hu, M., Liu, X., Mao, J., Sugimoto, N., and Wiedensohler, A.: Relationships between submicrometer particulate air pollution and air mass history in Beijing,
15 China, 2004–2006, Atmospheric Chemistry and Physics, 8, 6155–6168, 2008.

WHO: Air quality guidelines for Europe, 2nd Edn., Copenhagen, World Health Organization Regional Office for Europe, WHO Regional Publications, European Series No. 91, 2000.

World Health Organization (WHO), Ambient (outdoor) air pollution in cities database. http://www.who.int/phe/health_topics/outdoorair/databases/cities/en/, 2014-07-05.

20 Wiedensohler, A., Birmili, W., Nowak, A., Sonntag, A., Weinhold, K., Merkel, M., Wehner, B., Tuch, T., Pfeifer, S., Fiebig, M., Fjäraa, A. M., Asmi, E., Sellegri, K., Depuy, R., Venzac, H., Villani, P., Laj, P., Aalto, P., Ogren, J. A., Swietlicki, E., Williams, P., Roldin, P., Quincey, P., Hüglin, C., Fierz-Schmidhauser, R., Gysel, M., Weingartner, E., Riccobono, F., Santos, S., Grüning, C., Faloon, K., Beddows, D., Harrison, R., Monahan, C., Jennings, S. G., O'Dowd, C. D., Marinoni, A., Horn, H.-G.,
25 Keck, L., Jiang, J., Scheckman, J., McMurry, P. H., Deng, Z., Zhao, C. S., Moerman, M., Henzing, B., de Leeuw, G., Löschau, G., and Bastian, S.: Mobility particle size spectrometers: harmonization of technical standards and data structure to facilitate high quality long-term observations of atmospheric particle number size distributions, Atmospheric Measurement Techniques, 5, 657–685, 2012.

Wu, Z. J., Hu, M., Lin, P., Liu, S., Wehner, B., and Wiedensohler, A.: Particle number size distribution
30 in the urban atmosphere of Beijing, China, Atmospheric Environment, 42, 7967–7980, 2008.

Zhai, S. X., Jacob, D. J., Wang, X., Shen, L., Li, K., Zhang, Y. Z., Gui, K., Zhao, T. L., and Liao, H.:
Fine particulate matter (PM$_{2.5}$) trends in China, 2013–2018: separating contributions from
anthropogenic emissions and meteorology, Atmospheric Chemistry and Physics, 19, 11031–11041,
2019.

5   Zhao, H. J., Gui, K., Ma, Y. J., Wang, Y. F., Wang, Y. Q., Wang, H., Zheng, Y., Li, L., Zhang, L., Che, H.
Z., and Zhang, X. Y.: Climatology and trends of aerosol optical depth with different particle size and
shape in northeast China from 2001 to 2018, Science of the Total Environment, 763, 142979, 2021.
Zhao, S. P., Yu, Y., and Qin, D. H.: From highly polluted inland city of China to "Lanzhou Blue": The
air-pollution characteristics, Sciences in Cold and Arid Regions, 10(1), 12–26, 2018.

10   Zhao, S. P., Yu, Y., Yin, D. Y., and He, J. J.: Meteorological dependence of particle number
concentrations in an urban area of complex terrain, Northwestern China, Atmospheric Research, 164–
165, 304–317, 2015a.
Zhao, S. P., Yu, Y., Xia, D. S., Yin, D. Y., He, J. J., Liu, N., and Li, F.: Urban particle size distributions
during two contrasting dust events originating from Taklimakan and Gobi Deserts, Environmental

15   Pollution, 207, 107-122, 2015b.
Zhao, S. P., Yu, Y., Yin, D. Y., He, J. J., Liu, N., Qu, J. J., and Xiao, J. H.: Annual and diurnal variations
of gaseous and particulate pollutants in 31 provincial capital cities based on in situ air quality
monitoring data from China National Environmental Monitoring Center, Environment International, 86,
92-106, 2016.

20   Zhao, S. P., Yu, Y., Yin, D., Yu, Z., Dong, L. X., Mao, Z., He, J. J., Yang, J., Li, P., and Qin, D. H.:
Concentrations, optical and radiative properties of carbonaceous aerosols over urban Lanzhou, a typical
valley city: Results from *in-situ* observations and numerical model, Atmospheric Environment, 213,
470-484, 2019.

25
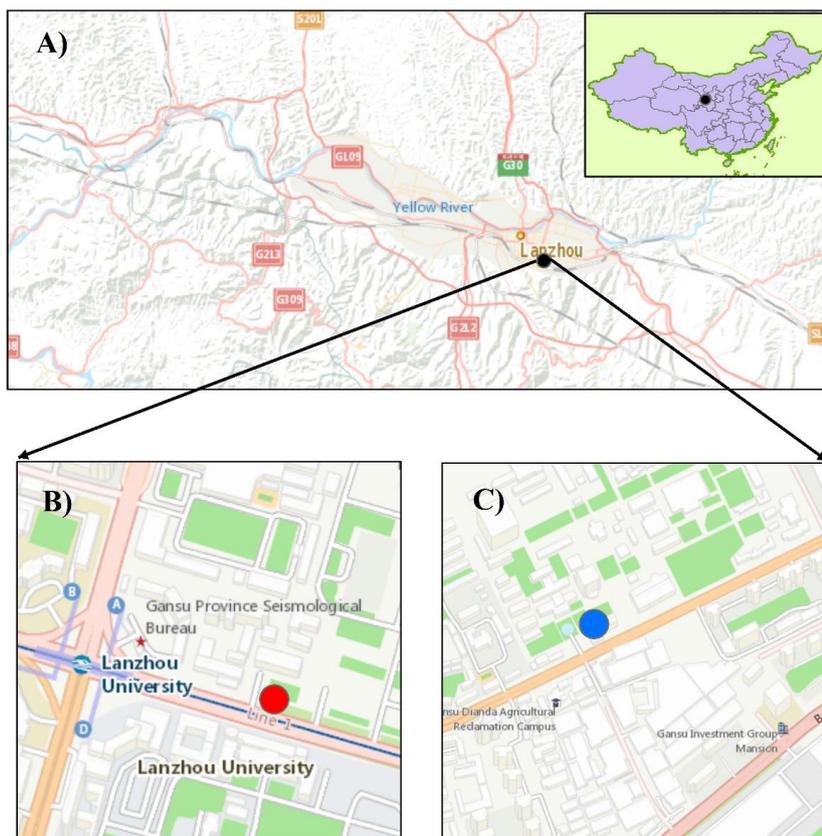
Figure 1: Map of A) Lanzhou City, B) the sampling site (red dot) and C) reference station that measured PM₂.₅ and O₃ (blue dot). The map is a pure reproduction of Google Maps where our own contribution is rather small, and we only added a few marks for our study locations.

5   **Copyright © Google Maps.**
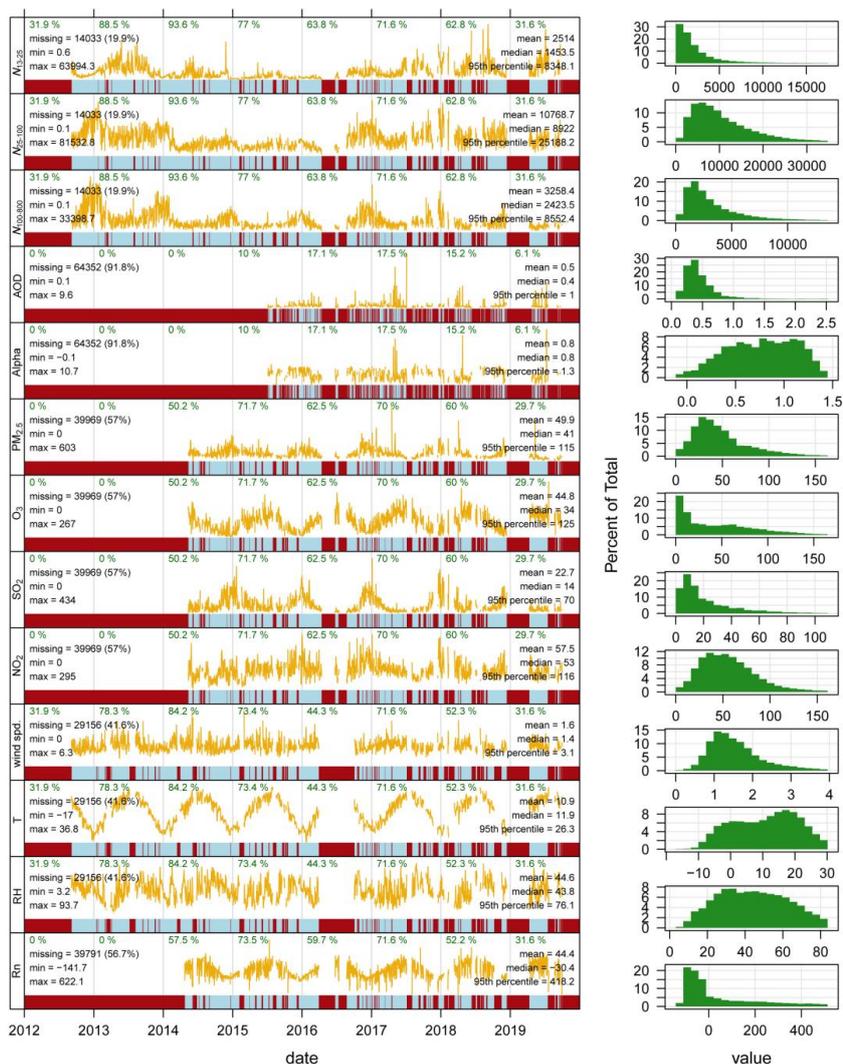
Figure 2: Time series of daily average particle number in the three modes (N_{13-25}, N_{25-100} and $N_{100-800}$), aerosol optical properties (AOD, Alpha), the criteria air pollutants (PM$_{2.5}$, O$_3$, SO$_2$, NO$_2$), and basic meteorological parameters and the corresponding probability density functions in urban Lanzhou during the campaign. The frequencies of missing values and the statistics are marked in each subplot. T, RH and Rn represent temperature, relative humidity and net radiation, respectively.
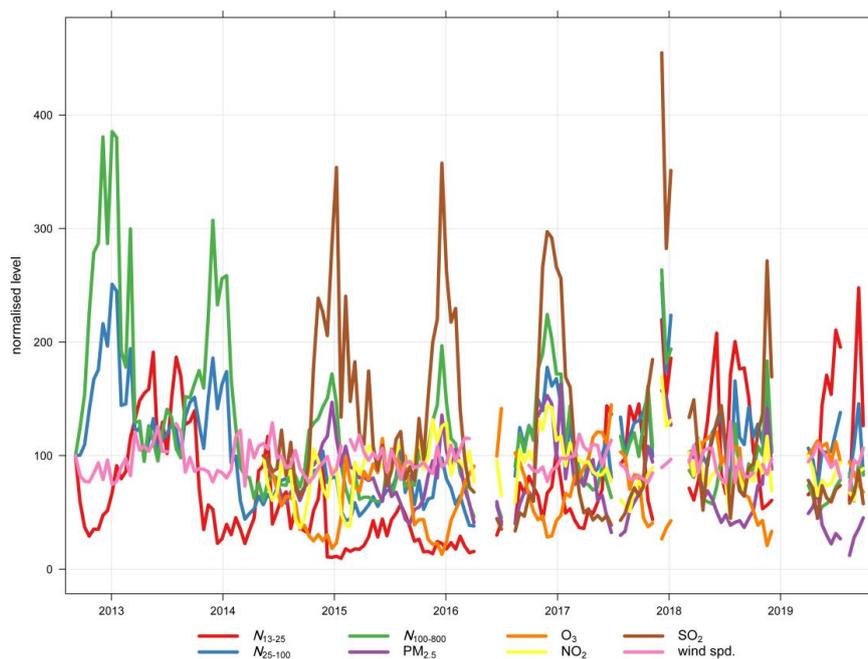
Figure 3: Normalizing time series of monthly averaged data (N_{13-25}, N_{25-100}, $N_{100-800}$, PM$_{2.5}$, O$_3$, NO$_2$, SO$_2$, wind speed) to fix values to equal 100 at the beginning of September 2012.
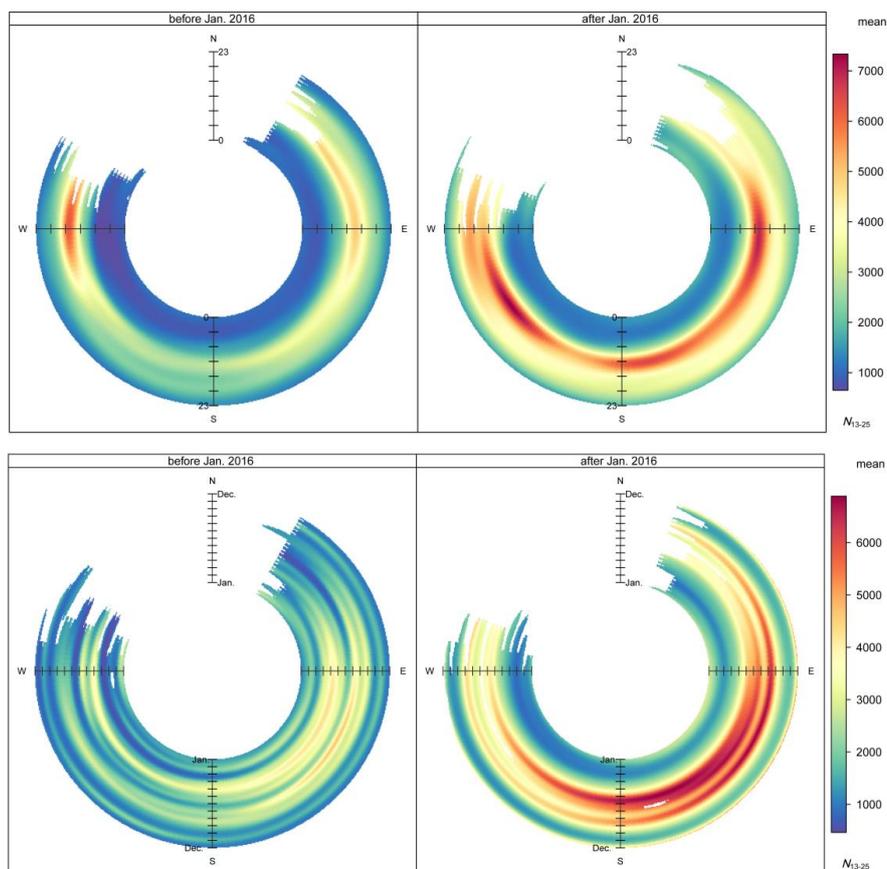
Figure 4: Mean diurnal (upper panel) and annual (lower panel) variations of particle number in 13-25 size bin (N_{13-25}) as wind directions before and after January 2016.
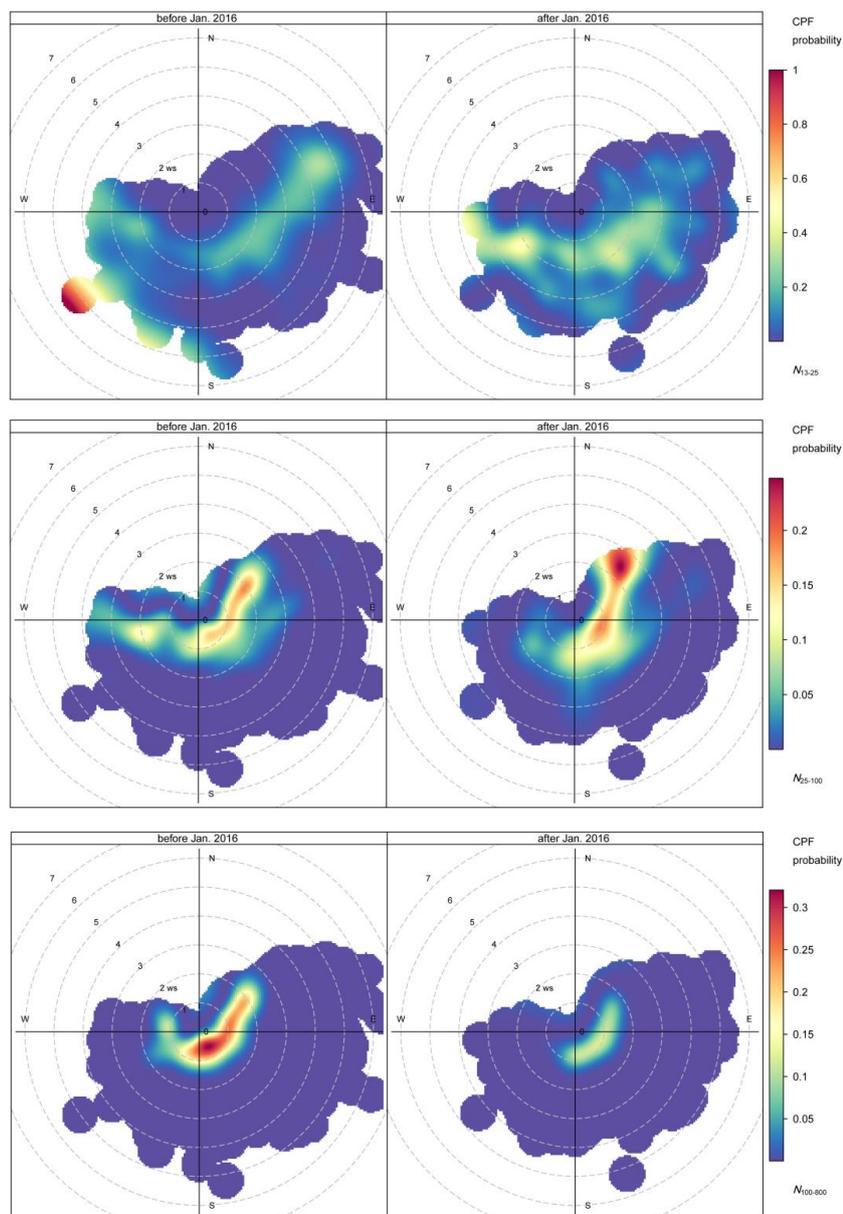
Figure 5: Polar plot of $N_{13\text{-}25}$ **(upper panel),** $N_{25\text{-}100}$ **(middle panel) and** $N_{100\text{-}800}$ **(lower panel) based on the CPF function before and after January 2016.**
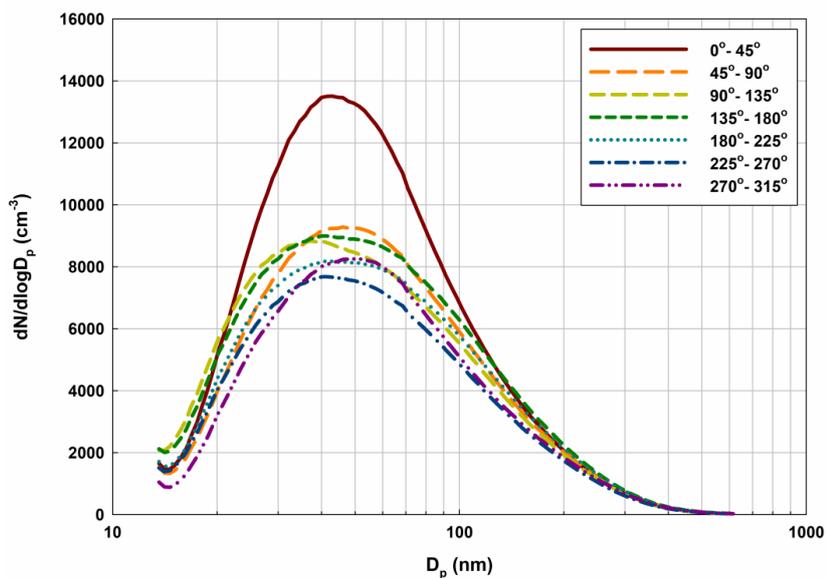
Figure 6: Mean particle number size distributions by each sector of wind directions with interval of 45 degree.
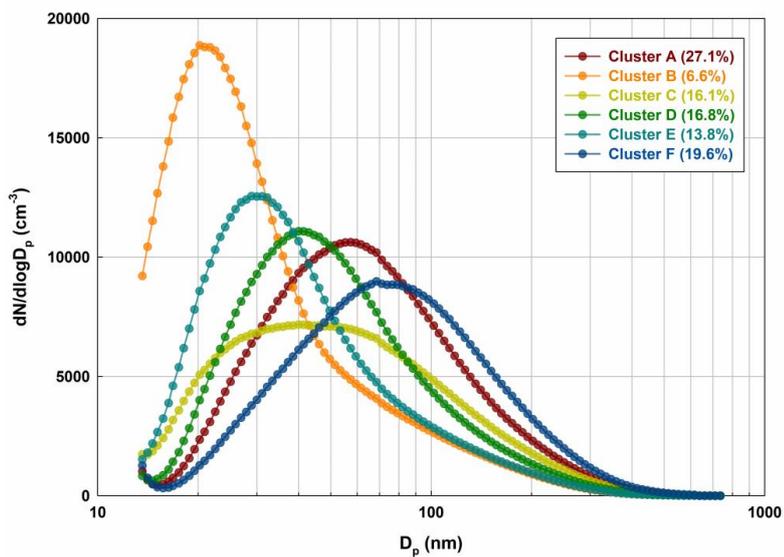
Figure 7: Mean particle number size distribution for each typical cluster obtained by K-means clustering method. The occurrence frequencies of Clusters A-F were calculated during 2012-2019.
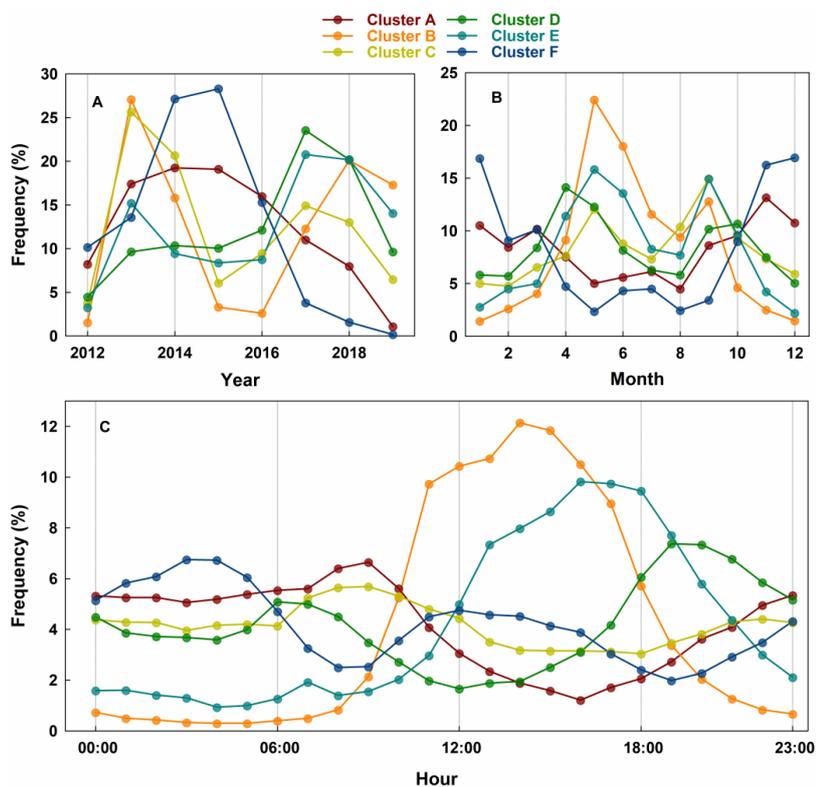
Figure 8: (A) Inter-annual, (B) averagely annual and (C) diurnal variations of occurrence frequencies for Clusters A-F during the measurement campaign.
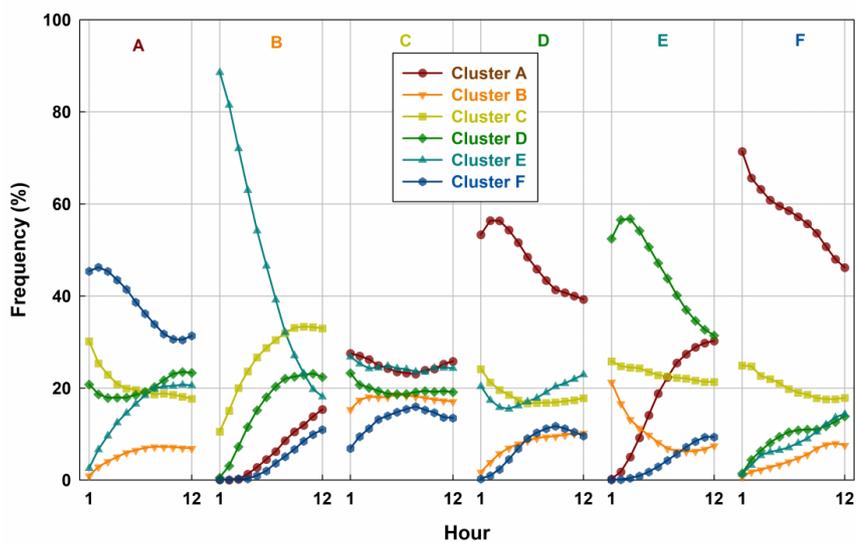
Figure 9: Occurrence frequency of Clusters A-F during 1-12 hours after each cluster appeared during the entire measurement campaign.
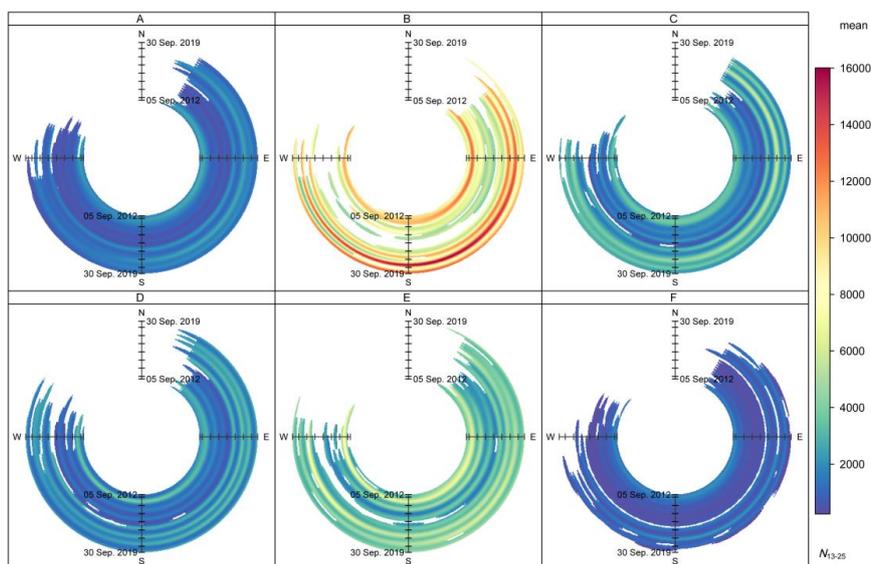
5   **Figure 10: Trends of daily mean number of particles in nucleation mode (N_{13-25}) as wind directions for each cluster during the entire measurement campaign.**
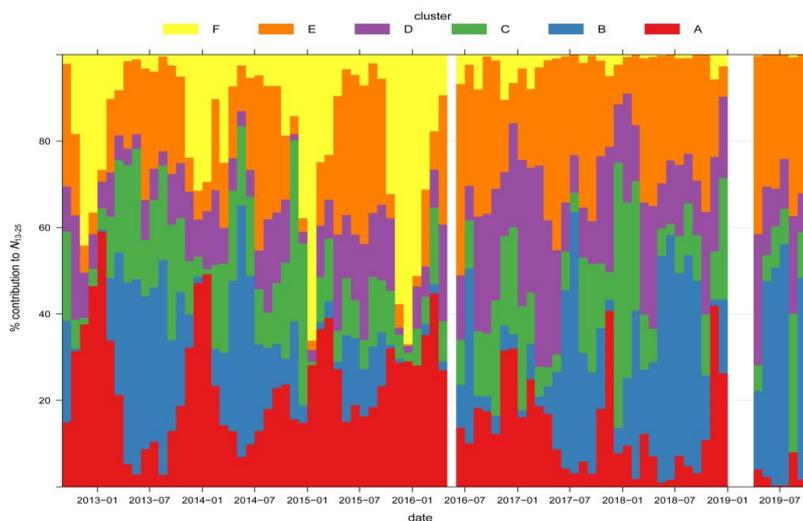
Figure 11: Variations of contribution of each cluster to monthly averaged N_{13-25} during the entire measurement campaign.
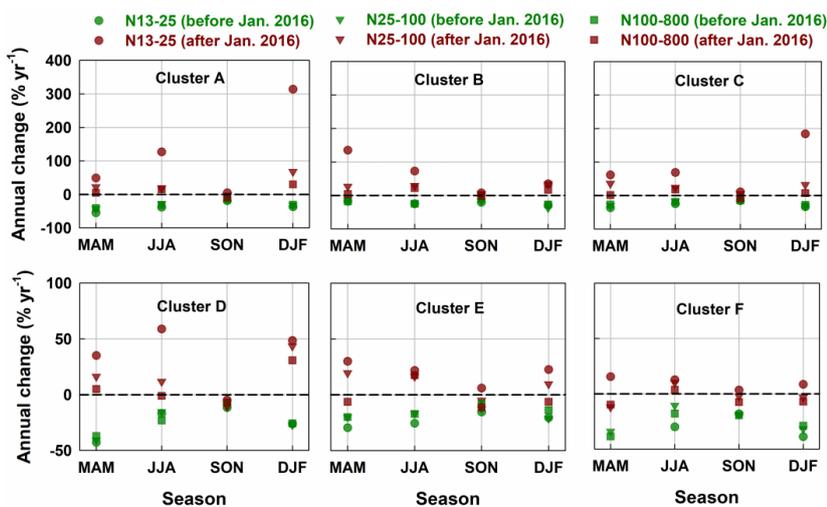
5 **Figure 12: Seasonal variations in the trends of PNCs in three modes before and after January 2016 for each cluster. The annual change is calculated by Theil-Sen regression. MAM, JJA, SON and DJF are spring, summer, fall and winter, respectively.**
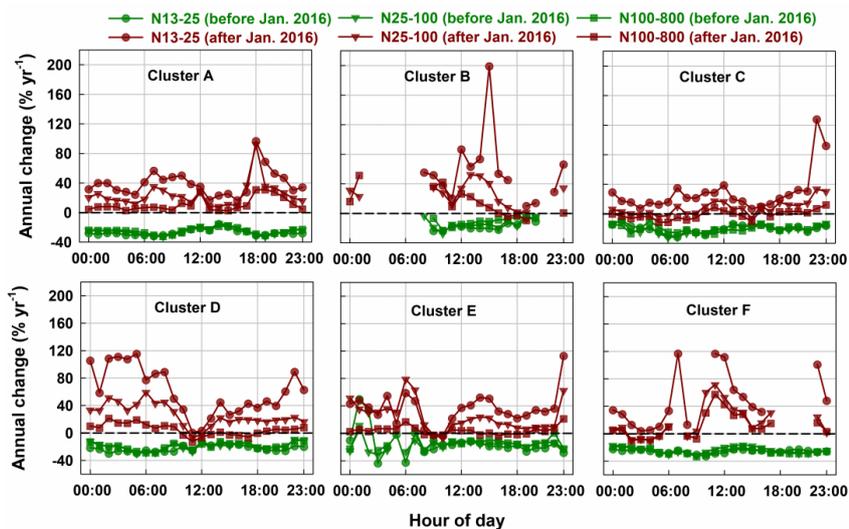
Figure 13: It is the same as Figure 12 but for diurnal variations.
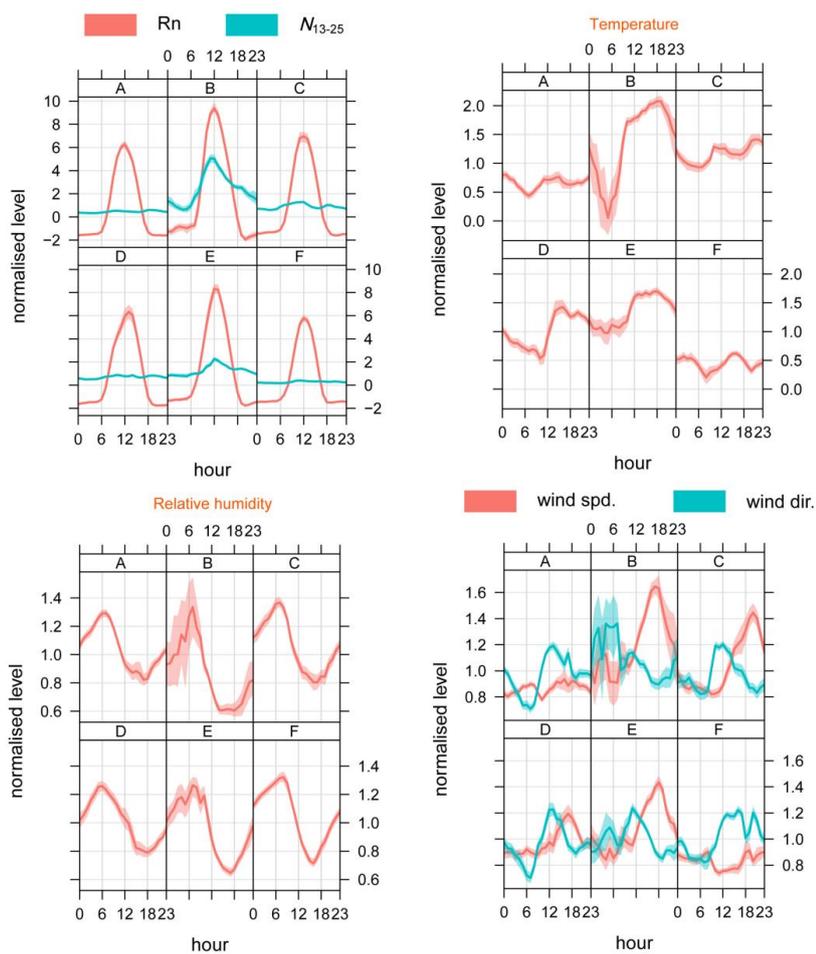
Figure 14: Normalized diurnal variations of net radiation (Rn), $N_{13\text{-}25}$, temperature, relative humidity, and wind speed and direction for each cluster. The shading shows the estimated 95% confidence intervals.

5
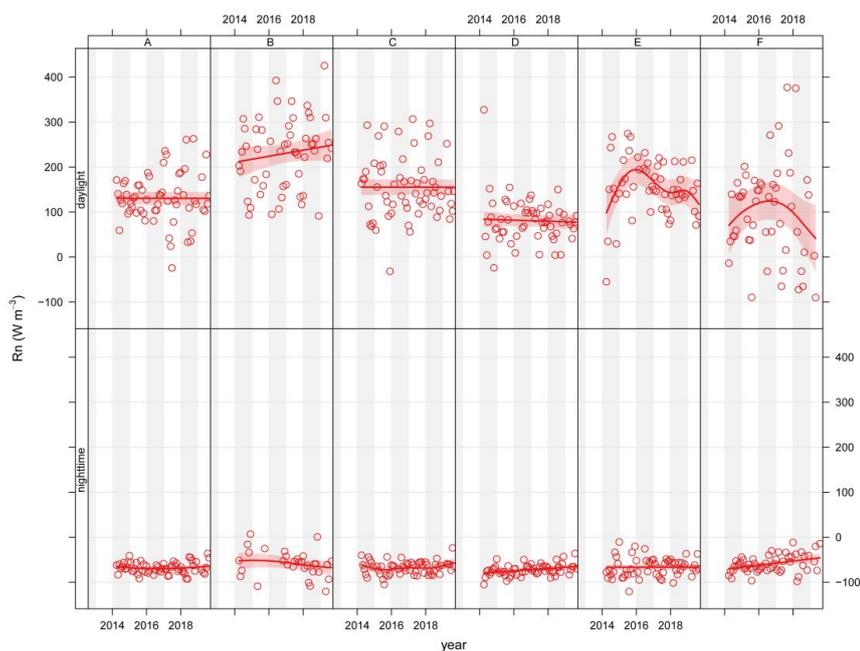
Figure 15: Inter-annual variations of monthly average daylight and nighttime Rn for each cluster during the campaign. The smooth line is essentially determined using Generalized Additive Model, and the shading shows the estimated 95% confidence intervals.

5
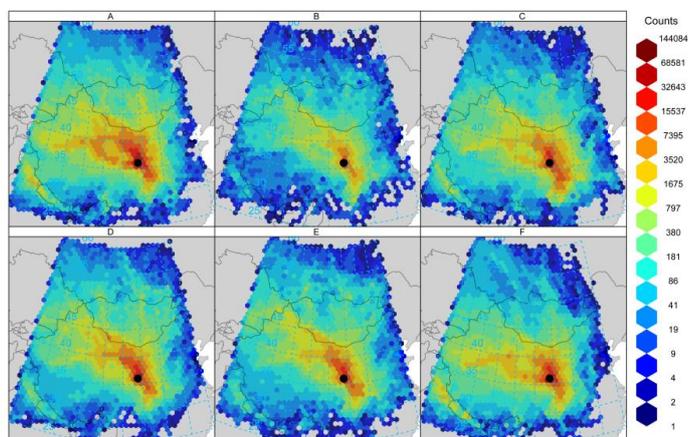
Figure 16: Gridded back trajectory frequencies with hexagonal binning for each cluster. The five-day (120 h) trajectories were initialized at 500 m AGL. The black dot shows the geographic location of urban Lanzhou.

Atmospheric
Chemistry
and Physics
Discussions
Open Access
EGU

Table 1. Overview of experimentally determined particle number concentrations in the troposphere around the world. The duration of the measurement campaign was at least longer than 1 year (12 months).

Continent	Diameter, city, site and period	Number concentrations			Reference
Asia	Diameter range (nm)	13-25	25-100	100-800	This work
	Lanzhou, urban, 7.5 years	2514	10769	3258	
	Diameter range (nm)	3-20	20-100	100-800	Wang et al. (2013)
	Beijing, urban, 3 years	5000	12300	6400	
	Diameter range (nm)	12-21	21-95	95-570	Kivekas et al. (2009)
	Waliguan, remote rural, 22 months	570	1060	430	
	Diameter range (nm)	3-25	25-100	100-1000	Shen et al. (2011)
	Shangdianzhi, rural, 1.5 years	3610	4430	3470	
	Diameter range (nm)		20-100	100-685	Kanawade et al. (2014)
	Kanpur, urban, 4 years		12400	18900	
	Diameter range (nm)	12-25	25-100	100-560	Gani et al. (2020)
	Delhi, urban, 1.25 years	8940	21690	11690	
Europe	Diameter range (nm)	8-25	25-90	90-460	Dal Maso et al. (2008)
	Varrio, rural, 3 years	143	429	304	
	Diameter range (nm)	8-30	30-100	100-700	von Bismarck-Osten et al. (2013)
	Copenhagen, rural, 3 years	770	1813	751	
	Diameter range (nm)	8-30	30-100	100-700	von Bismarck-Osten et al. (2013)
	Leipzig, roadside, 3 years	5692	4962	2242	
	Diameter range (nm)	8-30	30-100	100-700	von Bismarck-Osten et al. (2013)
	Helsinki, urban background, 3 years	3080	3099	1053	
	Diameter range (nm)	8-30	30-100	100-700	von Bismarck-Osten et al. (2013)
	London, urban background, 3 years	1632	3825	1437	
North America	Diameter range (nm)	10-50	50-100	100-500	Wang et al. (2011)
	Rochester, urban, 8 years	4730	1838	1073	
	Diameter range (nm)	3-20	20-100	100-1000	Stanier et al. (2004)
	Pittsburgh, urban, 1 year	9700	10100	2188	

5

Atmospheric
Chemistry
and Physics
Discussions

Table 2. Mean values of particle number in the three modes (N_{13-25}, N_{25-100}, and $N_{100-800}$), AOD, the concentrations of six criteria air pollutants (PM$_{2.5}$, PM$_{10}$, O$_3$, SO$_2$, NO$_2$, and CO) for each Cluster.

Cluster	N_{13-25}	N_{25-100}	$N_{100-800}$	AOD	PM$_{2.5}$	PM$_{10}$	O$_3$	SO$_2$	NO$_2$	CO
Units	cm^{-3}	cm^{-3}	cm^{-3}	—	µg m^{-3}	µg m^{-3}	µg m^{-3}	µg m^{-3}	µg m^{-3}	mg m^{-3}
A	1263.2	12156.5	3973.9	0.54	54.85	135.73	25.98	26.91	64.57	2.91
B	10370.4	9969.8	1504.7	0.39	31.42	86.53	92.77	13.56	40.67	2.73
C	2616.7	9071.8	2890.5	0.49	48.89	116.10	41.37	21.42	55.12	2.65
D	2010.0	11931.4	2301.6	0.55	43.92	124.13	46.28	16.85	57.68	2.33
E	4245.2	10806.9	1592.6	0.45	35.26	106.31	82.86	12.60	44.44	1.71
F	757.2	9492.2	5139.3	0.60	71.24	130.98	24.14	35.95	66.07	2.98

Table 3. Mean values of meteorological parameters (wind speed, temperature, relative humidity and net radiation) and geometric median diameters (GMD$_{nuc}$, GMD$_{Ait}$ and GMD$_{acc}$ are for nucleation, Aitken and accumulation modes) fitted by Eq. (1) for each Cluster. WS, T, RH, and Rn are the abbreviations of wind speed, temperature, relative humidity and net radiation, respectively.

Cluster	WS	T	RH	Rn	GMD$_{nuc}$	GMD$_{Ait}$	GMD$_{acc}$
Units	m s^{-1}	ºC	%	W m^{-2}	nm	nm	nm
A	1.38	7.35	48.39	21.56	26.37	54.91	133.08
B	2.18	20.77	31.59	223.55	19.72	38.06	131.70
C	1.64	13.18	48.20	48.25	22.56	49.91	137.21
D	1.57	11.73	44.31	-3.03	25.73	44.33	128.89
E	1.94	17.47	36.19	100.16	23.18	38.74	122.96
F	1.34	5.34	47.03	12.82	25.69	62.35	136.55